DOI: 10.26599/FSHW.2026.9251042

Contents lists available at SciOpen

Food Science and Human Wellness

journal homepage: https://www.sciopen.com/journal/2097-0765

China Food Publishing Co.

Synergistic Interactions of Polymerized Whey Protein and Okra Polysaccharide: Combining Molecular Dynamics and Simultaneous Rheology and FTIR for Designing Enhanced Functional Goat Milk Yogurt with Sensory Profiling

Weibing Tao[a], Huiyu Xiang[a], Abbas Khan[b], Siyi Lv[a], Yanglin Nie[c], Lijun Guan[d], Kunlun Wang[d], Xiaomeng Sun[a,e]*, Chun Li[a,f]*

[a]*Key Laboratory of Dairy Science, College of Food Science, Northeast Agricultural University, Harbin, Heilongjiang 150030, China.*

[b]*University of Home Economic Lahore Pakistan.*

[c]*Jiangsu Aimu Nutrition Technology Co., LTD, Huaian, Jiangsu, 211616, China.*

[d]*Food Processing Institute, Heilongjiang Academy of Agricultural Sciences, Harbin 150000, China.*

[e]*Danisco (China) Co. LTD, Kunshan, Jiangsu, 215300, China.*

[f]*China Heilongjiang Green Food Research Institute, Harbin 150028, China.*

ABSTRACT: The present study aimed to investigate the gel characteristics of hydrogels formed by 10% (w/v) polymerized whey protein (PWP) and 0-0.75% (w/v) okra polysaccharide (OPS) through heat-induced gelation. The potential application of these hydrogels as thickening agents in goat yogurt was also assessed. Results demonstrated that the addition of OPS promoted the formation of a stable three-dimensional network structure in the PWP-OPS hydrogels, mediated by hydrogen bonding and hydrophobic interactions. Simultaneous rheology and FTIR spectroscopy analysis revealed conformational changes and the burial of aromatic amino acid residues during the heating process. Molecular docking and molecular dynamics simulations further confirmed the spontaneous polymerization and stable complex formation between PWP and OPS. The PWP-OPS hydrogels exhibited superior physicochemical properties and gelation characteristics compared to the individual components. When applied in goat milk yogurt, the incorporation of 1% PWP-OPS hydrogel (comprising 10% PWP and 0.75% OPS) significantly improved ($P < 0.05$) the texture, sensory attributes, and microstructure, as determined by texture profile analysis, electronic nose and tongue, and scanning electron microscopy. These findings provide a fundamental theoretical basis for the development and application of protein-polysaccharide hydrogels in dairy products.

Keywords: PWP-OPS hydrogel, Simultaneous rheology and FTIR spectroscopy, Molecular dynamics, Goat yogurt, Electronic nose and tongue

1. Introduction

Goat milk is relatively superior to cow's milk and has multiple functional characteristics, e.g., promoting digestion, improving gastrointestinal function, having low allergenicity, and facilitating the absorption of minerals [1–4]. In addition, goat milk is rich in high biological value proteins, essential fatty acids, high mineral bioavailability, and vitamins [5]. However, the current market share of goat milk yogurt is relatively

***Corresponding author**
sunxm@neau.edu.cn, lchun@neau.edu.cn

Received 11 August 2025
Received in revised from 31 October 2025
Accepted 20 November 2025

small. This is because the output of goat milk is less than that of cow milk [6]. The more important reason is that the texture of goat milk yogurt, such as hardness, consistency, cohesiveness, and viscosity index, is extremely poor and far inferior to that of cow milk yogurt [2,7–9]. Therefore, it is necessary to study a new type of substance to improve the texture of goat milk yogurt.

In food industries, hydrogels are often added as thickeners [10]. The properties of hydrogels can be enhanced through the integration of proteins and polysaccharides [11]. Ban et al. [12] found that non-fat yogurt could significantly enhance the quality by adding WPI-mogroside hydrogels. Therefore, it can be concluded that hydrogel can improve the texture of yogurt.

Whey protein isolate (WPI), the primary component of which is β-lactoglobulin [13], is a dairy by-product with unique nutritional and functional properties [14–16]. And WPI can form polymerized whey protein (PWP) under conditions such as heating [17,18]. The stability of individual PWP remains a significant challenge, limiting their application in goat milk yogurt [19]. Existing research has demonstrated that the incorporation of polysaccharides as composite components can effectively enhance the stability of hydrogel structures [20,21].

Okra is a widely available vegetable with rich sap. Okra polysaccharide (OPS) is the main active substance of okra [22] and is often regarded as rhamnogalacturonan-I-type polysaccharide [23]. Due to well-established extraction techniques, OPS benefits from high output and low production costs. This makes it a promising candidate for widespread application in the food processing industry. Liao et al. [24] found that OPS could reduce lipid accumulation and improve lipotoxicity. In the food field, OPS can improve gel properties, which could affect the water retention of the gel to make the gel more elastic and viscous [25]. However, the synergistic interactions between PWP and OPS, particularly at a molecular level, remain poorly understood. Most existing studies focus on empirical observations of gel properties, lacking a mechanistic explanation that integrates real-time structural evolution during gelation with computational simulations to elucidate the binding dynamics and stability of the complex.

The novelty of this study lay in the multi-scale and interdisciplinary approach employed to decipher the PWP-OPS interactions and their application. Specifically, for the first time, simultaneous rheology and FTIR (SR-IR) coupled with two-dimensional correlation spectroscopy (2D-COS) were employed to monitor the heat-induced gelation process in real time, enabling the identification of the sequence and sensitivity of functional group changes under temperature perturbation. The findings from SR-IR/2D-COS were further integrated with molecular docking and dynamics simulations, providing atomic-level insight into the binding mechanisms, stability, and conformational changes underlying the PWP-OPS complex formation, thereby bridging macro-scale properties with nano-scale interactions. Moreover, the application of the optimized PWP-OPS hydrogel in goat milk yogurt was comprehensively evaluated, demonstrating significant improvements not only in texture and water-holding capacity but also in sensory profile and antioxidant properties. This study thus provides a theoretical foundation and practical strategy for developing high-quality functional dairy products.

This study characterized the physicochemical properties of PWP-OPS hydrogel and assessed its subsequent effects on the texture and sensory qualities of goat milk yogurt. Molecular-level interactions between OPS and PWP, including hydrogen bonding, covalent linkages, and hydrophobic associations, were characterized using SR-IR, molecular docking, and molecular dynamics simulations. Two-dimensional correlation spectroscopy and cryogenic scanning electron microscopy further elucidated the structural changes during PWP-OPS hydrogel formation. The effects of incorporating the PWP-OPS hydrogel on yogurt texture, volatile profile, and taste were also evaluated. The findings provide valuable insights into the potential application of the PWP-OPS complex as a functional food ingredient to enhance the quality attributes of goat milk yogurt.

2. Materials and Methods

2.1. Materials

The WPI powder (93.14% purity) was obtained from Fonterra (Auckland, New Zealand). The Okra polysaccharide (OPS, 90% purity, molecular weight range from 6,436 to 7,432 kDa) was purchased from Xi'an Baoyifeng Biological Technology Co., Ltd. 2,2-Diphenyl-1-picrylhydrazyl (DPPH) and 2,2′-Azino-bis (3-ethyl-benzothiazoline-6-sulfonic acid) diammonium salt (ABTS) were acquired from Beijing Bio-Tech Co., Ltd. 5,5′-Dithiobis (DTNB), 8-Anilino-1-naphthalenesulfonic acid (ANS), ABY-8 (leavening agent), and goat milk powder were obtained from Beijing Boao Tuoda Technology Co., Ltd, Macklin Biochemical Technology Co., Ltd, Danisco (China) Co., Ltd, and Beijing Zhongtian Xuteng Food Co., Ltd, respectively. All other chemicals used were of analytical grade.

2.2. Preparation of hydrogels

2.2.1. Preparation of WPI-OPS samples

Separate 20% (w/v) WPI and 6% (w/v) OPS stock solutions were prepared by dissolving the respective powders in deionized water and refrigerating overnight at 4℃. The WPI and OPS solutions were then combined to obtain final WPI concentrations of 10% (w/v) and OPS concentrations of 0.1%, 0.25%, 0.5%, and 0.75% (w/v).

2.2.2. Preparation of PWP-OPS composite hydrogels

The pH of the WPI-OPS samples was adjusted to 7.00 using 1 M NaOH. Heat-induced WPI-OPS was prepared by heating 50 mL aliquots of the WPI-OPS solutions in 50 mL beakers, which were covered with cling film to prevent moisture loss. The samples were heated in a magnetic stirring water bath at 85℃ for 30 min with gentle agitation. Afterwards, the samples were cooled to 25℃ at room temperature.

2.3. Preparation of Yogurt

Goat yogurts were prepared with varying levels of PWP-OPS hydrogels. Group A served as the control, comprising goat yogurt without PWP or PWP-OPS hydrogel. Groups B-F contained goat milk supplemented with 1% hydrogels, with OPS concentrations ranging from 0 to 0.75% (w/v), respectively. (The exclusion of 1% OPS and 10% PWP in the formulation was due to the formation of a water-insoluble complex between

PWP and OPS when OPS was added at a concentration of 1%, rendering it unsuitable for inclusion in yogurt (Fig. S1). The goat milk was reconstituted from 13.5% goat milk powder in deionized water, heated to 40℃, and supplemented with 7% (w/v) sugar. Pasteurization was achieved by heating the milk to 85℃ for 30 min. The milk was then cooled to 42℃, inoculated with 0.03% ABY-8 fermentation starter, and combined with 1% PWP-OPS hydrogels (containing 10% PWP and 0-0.75% OPS). Fermentation proceeded at 42℃ until the pH reached 4.5. Finally, the goat yogurt was cooled and stored at 4℃ for further analysis [26].

2.4. Size and zeta potential measurements

2.4.1. Micrometer particle size measurement

The particle size distribution of the goat milk yogurt was analyzed using a Malvern 3000 laser diffraction particle sizer (Mastersizer3000E, Malvern, England) [27,28].

2.4.2. Nanoparticle size measurement and Zeta potential measurement

The hydrodynamic size of the solution samples was determined using a Zetasizer Nano ZS (Malvern Instruments, Worcestershire, UK) [29], as per the protocol described by Zhao et al. [30] with minor modifications. The PWP-OPS were diluted 100-fold prior to analysis.

2.5. Rheological tests

2.5.1. Apparent viscosity and Modulus test

The apparent viscosity of hydrogel and yogurt samples was measured using a Rheonaut Rheometer (Thermo Scientific HAAKE, MARS 40, USA). A 10 mL aliquot of the sample was added to the 30 mm lower plate, and the upper plate had a diameter of 30 mm. Measurements were conducted at 25℃ with a shear rate range of 10-600 s^{-1}, and the apparent viscosity was recorded at a shear rate of 100 s^{-1} [31]. The modulus was assessed by scanning samples at frequencies from 0.1 to 10 Hz at 25℃, using 30 mm parallel plates. Storage modulus (G') and loss modulus (G") results were documented [32].

2.5.2. Dynamic rheology

The upper plate had a diameter of 60 mm. Subsequently, 10 mL of an OPS-WPI solution was added to the lower plate, which had a diameter of 60 mm. Silicone oil was then applied around the sample to prevent evaporation, and a thermal insulation cover was added. The determination gap was set to 0.8 mm in the software, and the temperature was increased from 25℃ to 85℃ at a rate of 5℃/min, maintained at 85℃ for 30 min, and then cooled back to 25℃ at a rate of 1℃/min, with a strain of 0.1%. The relationship between the G" and G' of the sample and the angular frequency was determined at 85℃ within the frequency range of 0.1 - 25 Hz [33].

2.6. Antioxidant properties

The antioxidant activities were evaluated using the DPPH and ABTS assays, following established protocols [34,35]. For the DPPH assay, a 0.08 mM DPPH solution was prepared by dissolving 6.3 mg of DPPH powder in 200 mL of absolute ethanol under dark conditions. A 0.5 mg/mL sample solution was mixed with the DPPH solution in a 1:1 ratio and allowed to react for 30 min in the dark at room temperature.

The absorbance was then measured at 517 nm using a UV-vis spectrophotometer. The ABTS assay involved generating the ABTS radical cation by mixing equal volumes of ABTS (7 mM) and potassium persulfate (2.45 mM) and allowing the reaction to proceed for 16 h in the dark at room temperature. The ABTS solution was diluted with ethanol until the absorbance at 734 nm reached 0.70±0.02. A 0.5 mg/mL sample solution was mixed with the diluted ABTS solution in a 1:6 ratio and incubated for 6 minutes in the dark at room temperature before measuring the absorbance at 734 nm. A control was prepared by mixing the sample solution with phosphate-buffered saline (PBS). The free radical scavenging ability was calculated using the following formula:

$$\text{Free radical scavenging rate} / \% = (1 - \frac{A_i - A_j}{A_0}) \times 100\% \quad (1)$$

The ABTS and DPPH assays employed distinct methodologies to assess antioxidant capacity. In the ABTS experiment, A_i represents the absorbance of the diluent-ABTS solution mixture, while in the DPPH experiment, A_i corresponds to the absorbance of the diluent-DPPH solution mixture. A_j denotes the absorbance of the 0.5 mg/ml sample dilution-PBS solution mixture for ABTS, and the absorbance of the 0.5 mg/ml sample dilution-absolute ethanol mixture for DPPH. A_0 signifies the absorbance of the deionized water-ABTS working solution mixture for ABTS, and the absorbance of the deionized water-DPPH solution mixture for DPPH.

2.7. Thermal stability measurement

The thermal stability of PWP-OPS was evaluated using differential scanning calorimetry (Mettler Toledo DSC 3, Zurich, Switzerland). An empty, sealed crucible served as the control. Approximately 5±0.5 mg of the freeze-dried PWP-OPS sample was heated from 25 to 200℃ [31].

2.8. Two-dimensional (2D) and Three-dimensional (3D) intrinsic fluorescence spectra and surface hydrophobicity

The fluorescence characteristics of PWP-OPS were examined using a F-4500 fluorescence spectrometer (Hitachi Ltd., Tokyo, Japan) with slight modifications from previous protocols. The 2D excitation wavelength was set to 280 nm, and the emission spectra were scanned from 290 to 400 nm with a 5 nm slit width. The 3D spectra were measured across an excitation wavelength range of 260 to 300 nm and recorded at emission wavelengths of 310 to 420 nm, with a 5 nm slit width and a 10 nm sampling interval [34,36].

Twenty microliters of ANS solution were added to 4 mL of a sample solution containing 10 mL per milliliter of protein, and the mixture was incubated in the dark for 15 min. The surface hydrophobicity of PWP-OPS was then measured using an F-4500 fluorescence spectrometer (Hitachi Co., Ltd., Tokyo, Japan). The excitation wavelength was set at 370 nm, and the emission spectra were recorded from 400 to 600 nm [37].

2.9. Free sulfhydryl

The free sulfhydryl content was determined using the method described by Zhang et al. [38]. The sample was diluted in a Tris-Gly buffer containing 4 mM EDTA, 90 mM Gly, and 86 mM Tris (pH 8.0). Ellman's reagent (50 μL) was added, and the solution was incubated for 30 min in the dark with shaking. The absorbance at 412 nm was then measured. The free sulfhydryl content was calculated accordingly.

$$\text{Free sulfhydryl content (μmol/g)} = \frac{73.53 \times A_{412} \times D}{C} \quad (2)$$

where D is the dilution factor, A_{412} is the absorbance at 412 nm, C represents the protein solution concentration (mg/mL), and 73.53 is the conversion factor for sulfhydryl concentration based on the molar extinction coefficient of the Ellman reaction.

2.10. Fourier transform infra-red spectroscopy (FTIR)

The FTIR spectra of the freeze-dried hydrogel samples were acquired using an infrared spectrometer (Nicolet iS10, Thermo Fisher Scientific, Germany). The measurements were recorded over the wavenumber range of 400 to 4000 cm^{-1}, with a total of 32 scans. The secondary structure of the protein was analyzed using the "Omnic" and "Peakfit" software, which employ a Gaussian peak fitting algorithm [17].

2.11. Simultaneous rheology (SR) and Fourier transform infrared (IR) spectroscopy (SR-IR) and its 2D correlation spectroscopy (2D-COS)

SR-IR was measured using the previously mentioned rheometer, equipped with a Nicolet iS10 spectrometer (Thermo Fisher Scientific, USA), following the methodology of Ban et al. [12]. Dynamic rheological measurements adhered to the protocol in section 2.4.2. FTIR spectra were recorded from 400 to 4000 cm^{-1}. Subsequently, 2D-COS was generated using the method of Xing et al. [34] with a plug-in in Origin 2024 software.

2.12. Determination of the pH of yoghurt during fermentation

The pH changes during yogurt fermentation were measured every 45 min using an INESA pH detector [32].

2.13. Water holding capacity (WHC)

The sample was centrifuged at 400 rpm for 20 min. The supernatant was discarded after inverting the centrifuge tube for 5 min [32]. The WHC was calculated using the formula:

$$\text{WHC}(\%) = \frac{m_1 - m_2}{m_1 - m_0} \times 100\% \quad (3)$$

where m_0 represents the weight of the empty centrifuge tube, m_1 represents the weight of the yogurt and centrifuge tube before centrifugation, and m_2 represents the weight of the yogurt and centrifuge tube after centrifugation.

2.14. Texture Profile

The texture of the yogurt samples was evaluated using a Texture Analyzer equipped with the TPA (Texture Profile Analysis) mode, following the protocol detailed by Zhu et al. [26]. The measurements were conducted with the following parameters: probe type: trigger force: 2 g; probe: AB-E/40; test speed: 1 mm/s;

test distance: 15 mm. The textural attributes assessed included gumminess, chewiness, cohesiveness, and hardness.

2.15. Electronic nose test

The yogurt was analyzed with an electronic nose (INSENT, Japan). A 5 g sample was placed in a 20 mL headspace vial and assessed at room temperature. The air flow rate was maintained at 300 mL/min for a duration of 60 s [39].

2.16. Electronic tongue test

The yogurt samples were analyzed using an electronic tongue (INSENT, Japan). The yogurt was diluted with deionized water at a 1:1 ratio and then centrifuged at 5,000× g for 10 min. The supernatant was further diluted with deionized water at a 1:10 ratio prior to measurement [40].

2.17. Microstructure

2.17.1. Cryogenic scanning electron microscopy (Cryo-SEM) of PWP-OPS

The microstructure of the PWP-OPS hydrogel samples was examined using a cryo-scanning electron microscope (SU8010, Hitachi Ltd., Japan). The samples were frozen in liquid nitrogen for 10 min and then fractured with a surgical blade to expose a cross-section. After etching at -85℃ for 20 min, the samples were sputter-coated with gold [41]. The microstructures were characterized at a magnification of 2500×.

2.17.2. Scanning electron microscopy (SEM) of yogurt

The microstructure of the yogurt was examined using a scanning electron microscope (S-3400N, Hitachi, Ltd., Japan) [42]. Samples were freeze-dried for 24 h using a freeze dryer (Alpha 1-4 LDplus, Martin Christ), then sputter-coated with gold, and observed at 2,500× magnification to obtain SEM images.

2.18. Molecular docking

The present study employed molecular docking to investigate the interaction between β-lactoglobulin, a major component of WPI [43], and oligosaccharides derived from OPS. The three-dimensional structure of β-lactoglobulin, obtained from the RSBC database, was prepared for docking using PyMOL software. OPS, previously characterized as a rhamnose-galacturonate-1 polysaccharide [23,44], was drawn in 2D and 3D using ChemDraw and Chem3D, respectively, and used as the ligand. Blind docking was performed using the CB-DOCK2 online server (https://cadd.labshare.cn/cb-dock2/php/blinddock.php), which utilizes artificial neural networks for cavity detection and Autodock Vina for the docking simulation [45]. The docking results were evaluated based on binding energy, and the binding stability was further assessed through force analysis and docking position evaluation. Ligand-receptor interactions were analyzed using the PLIP online server, and the 3D conformations of the ligand and receptor were visualized with PyMOL.

2.19. Molecular dynamics

Molecular dynamics simulations were employed to investigate the interaction between PWP-OPS [46]. The initial structure was based on the β-lactoglobulin-OPS complex from previous docking studies, and the

all-atom molecular dynamics simulations were carried out using the GROMACS 2023.3 software [47]. Both the small molecules and proteins were described using the AMBER force field [48,49]. The pdb2gmx subroutine was utilized to add hydrogen atoms to the system, and a truncated cubic TIP3P solvent box was introduced at a distance of 10 Å from the system, with Na^+/Cl^- ions added to neutralize the system charges [50]. The topology and parameter files for the simulation were then generated. The molecular dynamics simulation was performed for 100 ns using GROMACS 2023.3 software, and analyses were conducted on RMSD, RMSF, Rg, and the number of hydrogen bonds.

2.20. Statistical analysis

Experiments were conducted in triplicate, with results expressed as mean ± standard deviation. Data analysis and figure generation utilized IBM SPSS Statistics 26 (SPSS Inc., Chicago, USA) and Origin 2024 (OriginLab Corporation, Northampton, USA). Correlation analysis was performed using Origin 2024. [51].

3. Results and Discussion

3.1. Particle size of PWP-OPS

PWP-OPS hydrogels exhibited increased size with the increase in OPS level (Fig. 1A). The reason for the formation of this crosslink might be that hydrogen bonds have formed between PWP and OPS [26], leading to more OPS combining with PWP to form larger aggregates [52]. In addition, under infrared light exposure, a comparable scenario arose as the Tyndall effect progressively decreased (Fig. 1B). The weakening of light scattering was a direct consequence of the increased particle size and the formation of a coarser microstructure, which effectively obstructed the transmission of light [53,54]. Collectively, the particle size analysis and the Tyndall effect observation provided complementary evidence for the OPS-induced microstructural transition from a dispersed system to a more consolidated gel network.

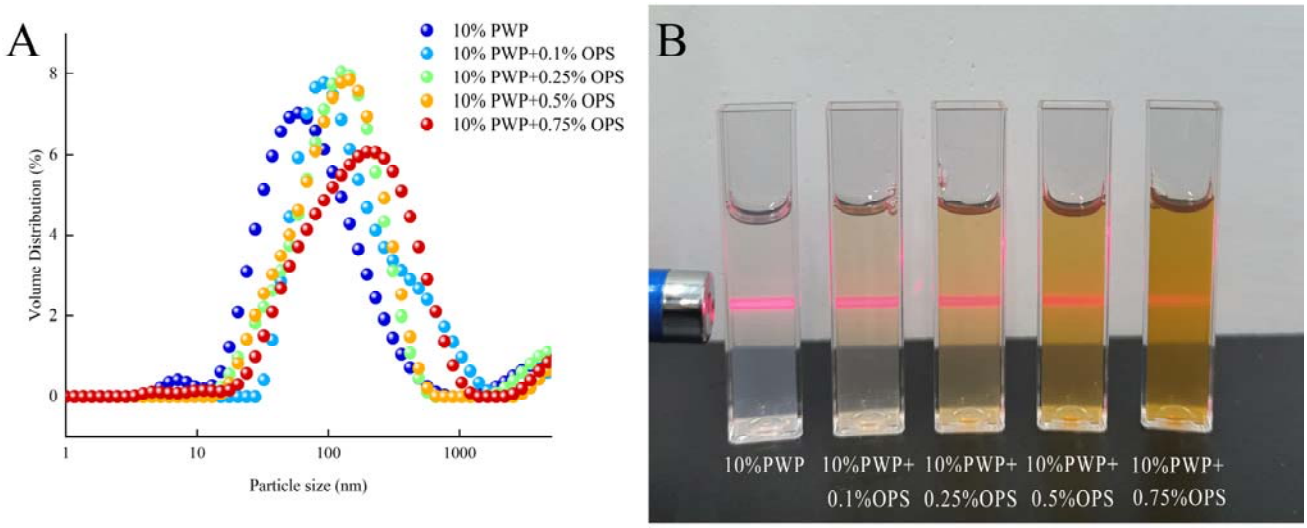

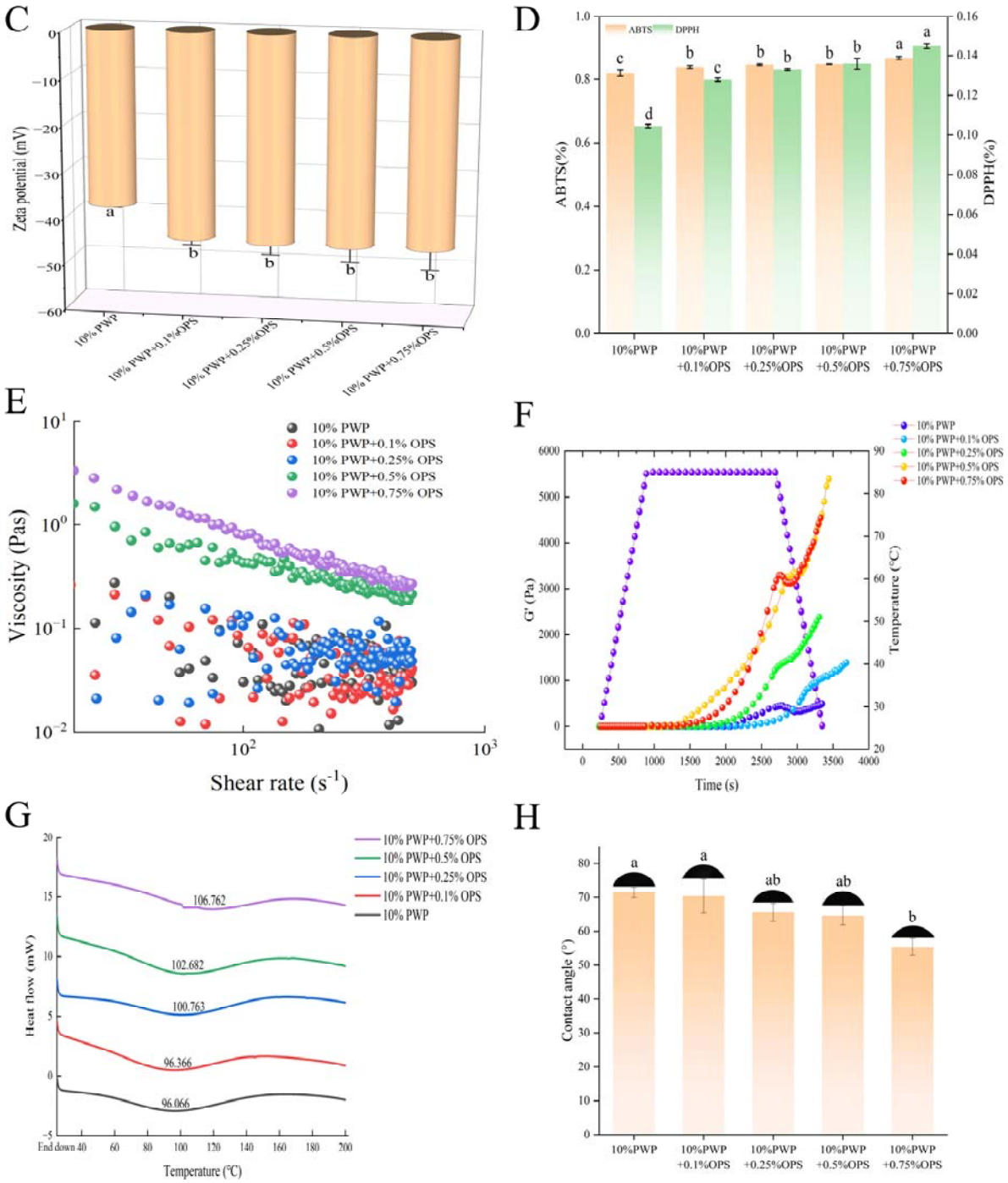

Fig. 1 Effect of OPS on the particle size (A), infrared laser irradiation (B), zeta potential (C), DPPH and ABTS (D), apparent viscosity (E), dynamic rheology (F), DSC curves (G) and water contact angle (H) of PWP-OPS with different OPS levels (0 - 0.75%, w/v)

3.2. Zeta potential of PWP-OPS

All samples exhibited a negative zeta potential, and the absolute zeta value increased significantly ($P < 0.05$) from 37.94 mV for PWP to 44.64 mV for PWP-OPS with 0.1% OPS (Fig. 1C). This could be attributed to the addition of OPS, which increased the electrostatic repulsion between PWP and OPS, disrupted the distance between PWP particles, and exposed more residues of the PWP structure. This facilitated improved binding and stabilization of OPS with PWP at a specific concentration [31,55,56]. An alternative explanation was that the molecular structure modification altered the orientation and

conformation of molecules at the solution interface, enhancing the overall negative charge of the system [27]. Specifically, the increased charge density strengthened electrostatic repulsion between the complexes, which initially disrupted the native PWP aggregate structure. This disruption, coupled with the potential shielding of positively charged groups on PWP by anionic OPS chains, led to a reorientation of molecules at the interface. Consequently, a greater proportion of anionic residues was exposed, facilitating the formation of a more stable complex through optimized electrostatic and non-covalent interactions.

3.3. Antioxidant property analysis

Free radical scavenging is a crucial measure for assessing shelf life and antioxidant properties. As shown in Fig. 1D, the free radical scavenging of PWP-OPS was improved by the increase in OPS levels, indicated by DPPH and ABTS values. It was possibly because of the antioxidant groups in OPS [22,23]. Additionally, the denser PWP-OPS network by OPS may also reduce oxygen transmission to slow down oxidation [57]. These characteristics suggest promising applications for PWP-OPS in yogurt.

3.4. Rheological properties of PWP-OPS

3.4.1 Apparent Viscosity

Apparent viscosity often indicates the frictional interaction intensity between polysaccharides and proteins [58]. The viscosity curve of the PWP-OPS hydrogel (Fig. 1E) showed a decrease in apparent viscosity with increasing shear rate, demonstrating shear-thinning or pseudoplastic behavior [59]. The apparent viscosity PWP-OPS hydrogel increased with the addition of OPS. The polyhydroxy nature of OPS could promote the formation of stable, dense electrostatic complexes with PWP to enhance shear resistance [60]. The specific viscosity properties of OPS may also prevent gel droplet movement and collision, decreasing emulsion fluidity and increasing apparent viscosity [61].

3.4.2. Dynamic rheology analysis

Dynamic rheology can effectively monitor changes in gel properties during heat treatment and predict gelation sites [62]. The G' assesses hydrogel network connectivity and cross-linking strength [63]. In PWP-OPS samples, G' increased with temperature and time (Fig. 1F), indicating hydrogel formation during heating. The G' value exceeding 1 Pa marks the gelation point where the complex transitions to a gel state [41]. As OPS content rose from 0% to 0.75%, gelation times for PWP-OPS hydrogels decreased from 2156 s to 2041 s, 1571 s, 108 s, and 966.1 s, respectively. OPS facilitated PWP-OPS hydrogel formation and strengthened PWP-OPS interactions, enhancing the hydrogel's elasticity and stability, thereby exhibiting solid-like behavior. The synergistic interplay of various physicochemical mechanisms underpinned the formation of PWP-OPS hydrogels with the increase in OPS concentration. Specifically, the enhanced hydrophobic cross-linking, thickening, and filling effects of polysaccharides, as well as the localized concentration driven by thermally-induced phase separation, collectively promoted hydrogel development. Furthermore, the elevated OPS levels furnished additional cross-linking sites for PWP, strengthening protein interactions and enabling specific binding to denatured protein functional groups (e.g., glutamine/amino

groups), thereby improving the overall hydrogel properties [64]. These findings aligned with the observations reported by Xiang et al. [31].

3.5. Differential scanning calorimetry (DSC) analysis

The endothermic peak observed around 100℃ (Fig. 1G) in the PWP curve was attributed to the protein denaturation [62]. With the increase in OPS content (0-0.75%), the heat absorption peak of PWP-OPS samples shifted to higher temperatures (from 96.066℃ to 106.762℃, which suggested that OPS could enhance the thermal stability of PWP hydrogel [30,65,66]. This was likely due to the increased hydrogen bonding interactions between PWP and OPS, which strengthened the thermal stability of the PWP-OPS system [26]. Furthermore, due to the molecular interaction between OPS and PWP, a dense and mutually permeable network structure was formed, which was beneficial for enhancing the overall stability of the gel [54,67].

3.6. 2D and 3D intrinsic fluorescence analysis

The intrinsic fluorescence of proteins can be attributed to the presence of aromatic amino acid residues, e.g., tyrosine, tryptophan, and phenylalanine [68,69]. The fluorescence intensity in 2D (Fig. 2A_1) and 3D (Fig. 2A_2-E_2) intrinsic fluorescence both gradually decreased with increasing OPS levels, which suggested a conformational change, where the aromatic amino acids became 'buried' and experienced fluorescence quenching [34,70]. The enhanced interaction between OPS and PWP could also be indicated [17] with the aromatic amino acids potentially transferring from the protein core to a more polar environment [52], reducing the amount of tryptophan residues in the non-polar environment in line with the findings of Xiang et al. [17] who reported a decrease in fluorescence intensity with the addition of fucoidan. Results suggested that the interaction between OPS and PWP leads to the formation of a more compact tertiary conformation [70,71], as further supported by the changes observed in the UV spectrum (Fig. 2C_1).

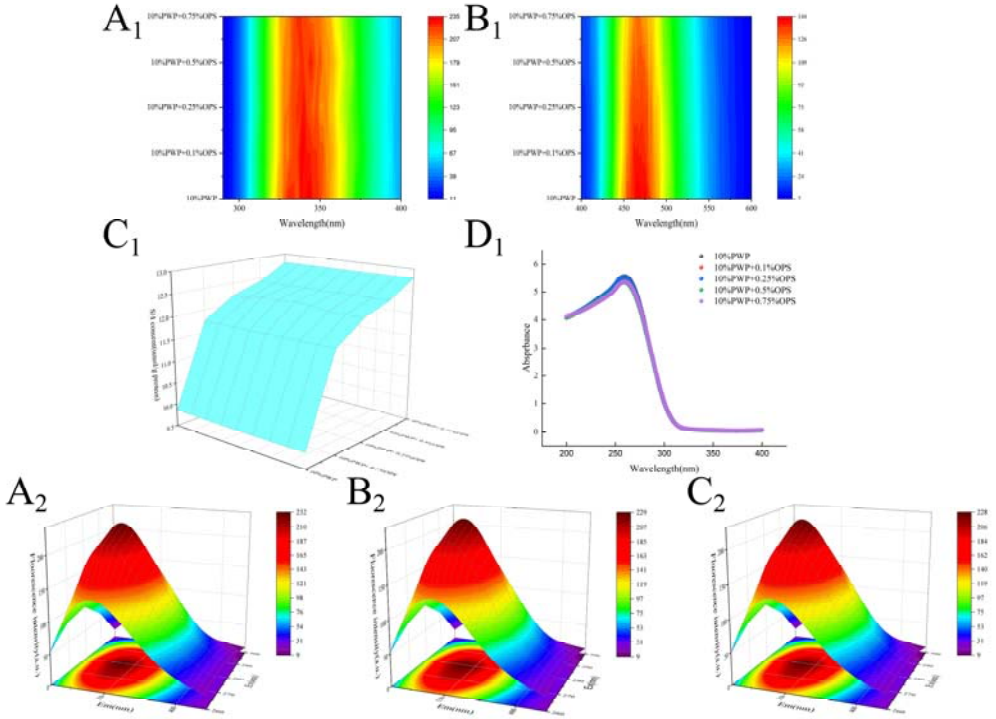

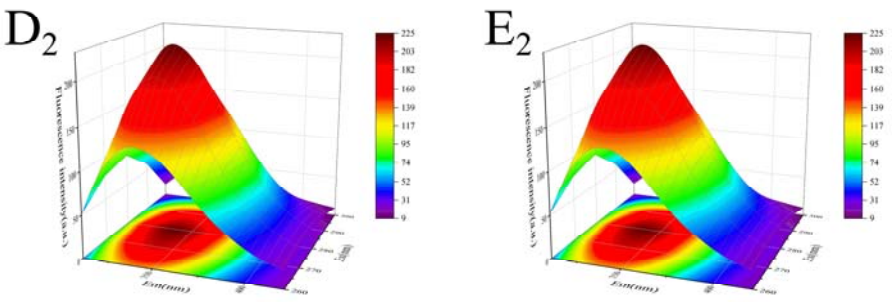

Fig. 2 Effect of OPS on the intrinsic fluorescence (A_1), surface hydrophobicity (B_1), ultraviolet spectrum (C_1), free sulfhydryl content (D_1), and 3D internal fluorescence spectrometry (A_2-E_2) of PWP-OPS with different OPS levels (0-0.75%, w/v)

3.7. Surface hydrophobicity analysis

The hydration forces are critical in preserving the tertiary structure of proteins [72]. The addition of OPS progressively reduced the surface hydrophobicity of PWP-OPS, reaching a minimum at 0.75% OPS (Figure 2B_1). This could be attributed to the enhanced electrostatic interaction between OPS and PWP, as well as the steric hindrance effect of OPS, which collectively inhibits the binding of the ANS probe to the protein's hydrophobic regions [73]. The incorporation of OPS increased the polarity of the solution [70], promoting backbone cross-linking between OPS and PWP molecules, thereby forming a more compact three-dimensional network structure and enhancing the interaction between hydrophobic groups [31]. The water contact angle data exhibited a consistent trend, indicating that the hydrophobicity of PWP-OPS diminished as OPS content increased (Fig. 1H).

3.8. Free sulfhydryl analysis

Disulfide bonds are crucial for maintaining the stable structure of the hydrogel, as evidenced by the changes in the content of free sulfhydryl groups in the protein [17]. The content of free sulfhydryl groups increased with the gradual increase in the OPS level (Figure 2D_1). Highly hydrophilic polysaccharides can convert water molecules into bound water, leading to an increase in the disulfide bond content in the protein system [74]. Additionally, heating and the addition of OPS might promote the expansion of whey proteins (such as β-lactoglobulin), exposing the internal hydrophobic regions, active sulfhydryl groups, and disulfide bond networks. Previous studies have shown that OPS can aggregate with PWP through hydrophobic interactions, resulting in a steric hindrance effect that hinders the formation of intermolecular disulfide bonds between free thiols [69].

3.9. SR-IR, secondary structure content and 2D correlation spectral analysis

3.9.1. SR-IR and 2D infrared spectrum analysis

The FT-IR spectra of PWP and PWP-OPS composite samples were shown in Fig. S2 and Fig. 3A_1-E_2. After adding different contents of OPS, the PWP-OPS hydrogels exhibited a specific absorption peak at the amide A band (3200 - 3400 cm^{-1}, N-H and O-H stretching vibration). The wavenumber corresponding to the characteristic peak of FTIR (Fig. S2) changed from 3288.04 to 3271.65, 3271.65, 3272.61 and 3272.61 cm^{-1}, respectively. And the wavenumber corresponding to the characteristic peak of 2D-FTIR (Fig. 3A_1-E_1)

changed from 3381 to 3374, 3381, 3380, and 3379 cm^{-1}. The position of the absorption peak moved to the direction of lower wavenumber. It was related to the stretching vibration of O-H, which indicated that PWP molecules and OPS molecules were associated with hydrogen bonds [52]. There was a small absorption peak around 3300 cm^{-1} in the 2D-FTIR of PWP-OPS samples, but it couldn't be found in PWP. This might be because the introduction of polysaccharides might lead to some slight fluctuation at this location [12]. The positions of FTIR absorption peaks in the amido I band (1700 - 1600 cm^{-1}, C=O tensile vibration) were 1625.22, 1625.22, 1625.22, 1625.70, and 1625.22 cm^{-1}, respectively. The second significant peak of 2D-FTIR mainly occurred in the amide I band at 1632.45, 1628.59, 1628.59, 1629.07, and 1632.45 cm^{-1}, respectively. The result indicated that OPS might change the stretching vibration frequency of C=O in PWP molecules due to the electrostatic attraction between PWP and OPS molecules. Similar to the results of Khan et al. [75], who reported that after embedding 3,3 '-diindolylmethane, the absorption peak in the amide I band of PWP implied the presence of intermolecular electrostatic attraction. Furthermore, the hydrogen bond formed by the graft of protein and polysaccharide might also reduce the stretching vibration frequency of C=O, according to Gao et al. [56]. The positions of the FTIR absorption peaks in the amide II band (1600-1500 cm^{-1}, C-N tensile vibration and N-H bending vibration) were 1512.40, 1512.40, 1513.85, 1512.88, and 1512.88 cm^{-1}, respectively [76]. It could be seen that the degree of absorption peak movement was not large, and it was caused by the stretching vibration of C=O as well as the N-H deformation vibration. In addition, after adding OPS to PWP with different mass ratios, the absorption peak of PWP at 1387.53 cm^{-1} moved to 1386.57, 1387.05, 1387.05 and 1386.57 cm^{-1}. It might be related to the symmetric deformation vibration of some alkyl groups and the change in hydrocarbon chain disorder. At the same time, with the addition of OPS, the absorption peak position of PWP in the fingerprint region moved from 1308.47 to 1307.98, 1307.98, 1307.50, and 1307.50 cm^{-1}, which was presumed to be related to C-O or C-N stretching vibration.

To analyze the final influence of heating treatment on the PWP-OPS samples, the first and last infrared spectra were separated from the SR-IR data (Fig. $3A_3$-E_3). During the heating process, there was an obvious peak around 3300 cm^{-1}, and the peaks shifted from 3269.23, 3353.60, 3280.32, 3269.23, and 3267.31 cm^{-1} to 3381.57, 3374.34, 3281.77, 3280.80, and 3379.64 cm^{-1}, respectively. The infrared spectra of PWP-OPS samples moved obviously in the direction of increasing wavenumber. This was because the coplanarity of aromatic amino acid residues conjugated systems was broken during the interaction of PWP and OPS molecules to form a hydrogel, causing the absorption peaks to shift towards a higher wavenumber. There was also a slight red shift in the amide I band. This might be attributed to the changes in the stretching vibration frequency of C=O in the PWP molecule during the heating process, which showed that the interaction between OPS and PWP might be caused by electrostatic attraction. Compared to PWP, the peak strength of PWP-OPS was significantly increased, suggesting that the addition of OPS led to greater disorder in the hydrocarbon chains. This suggested that the secondary structure of PWP-OPS changed during the heating process [12].

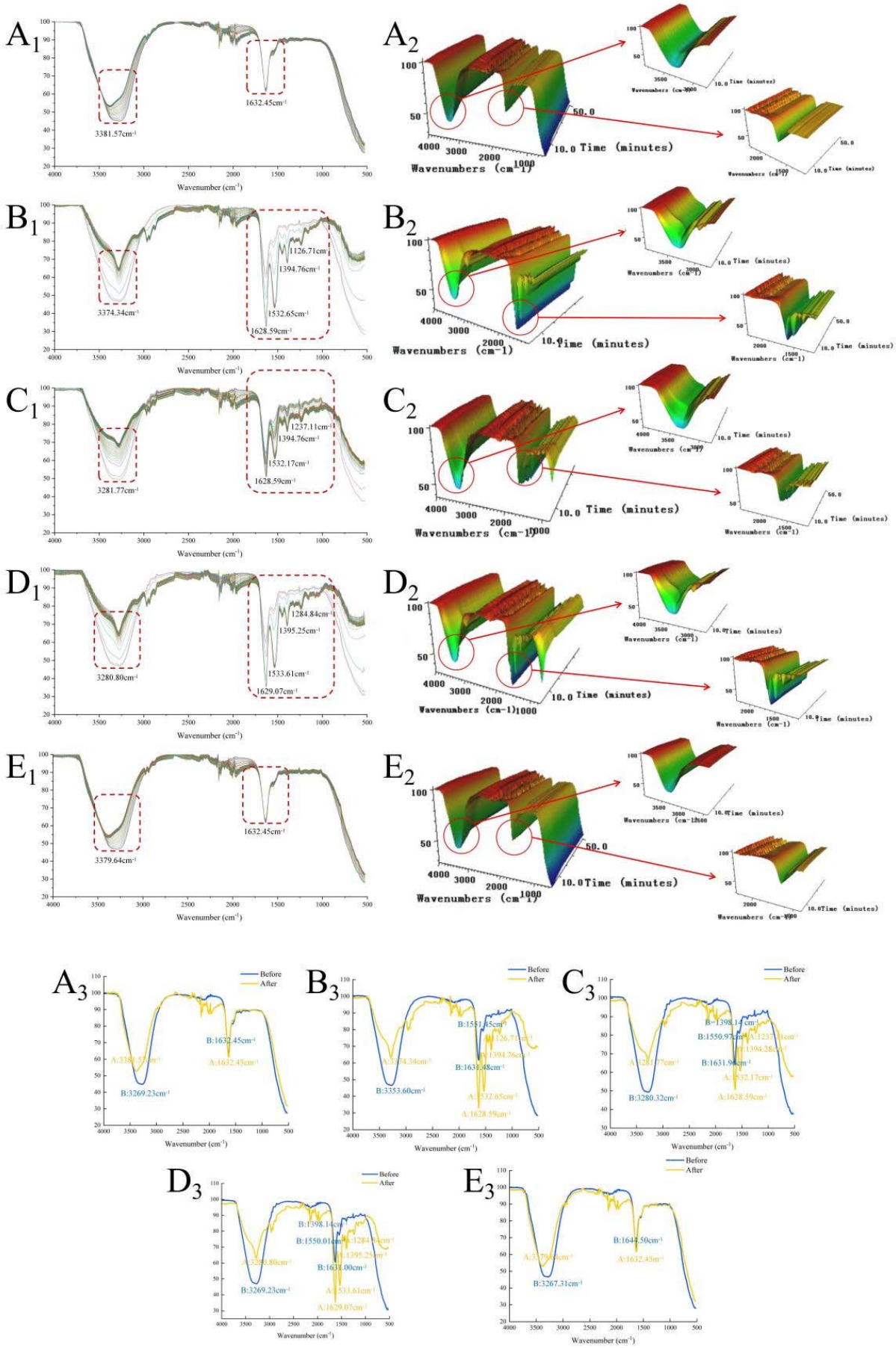
A1
3381.57cm-1
1632.45cm-1
Wavenumber (cm-1)
A2
Wavenumbers (cm-1)
Time (minutes)
B1
3374.34cm-1
1126.71cm-1
1394.76cm-1
1532.65cm-1
1628.59cm-1
B2
C1
3281.77cm-1
1237.11cm-1
1394.76cm-1
1532.17cm-1
1628.59cm-1
C2
D1
3280.80cm-1
1284.84cm-1
1395.25cm-1
1533.61cm-1
1629.07cm-1
D2
E1
3379.64cm-1
1632.45cm-1
E2
A3
Before
After
B:3269.23cm-1
B:1632.45cm-1
B3
B:3353.60cm-1
B:1631.48cm-1
C3
B:3280.32cm-1
B:1631.98cm-1
D3
B:3269.23cm-1
B:1631.00cm-1
E3
B:3267.31cm-1
B:1644.50cm-1

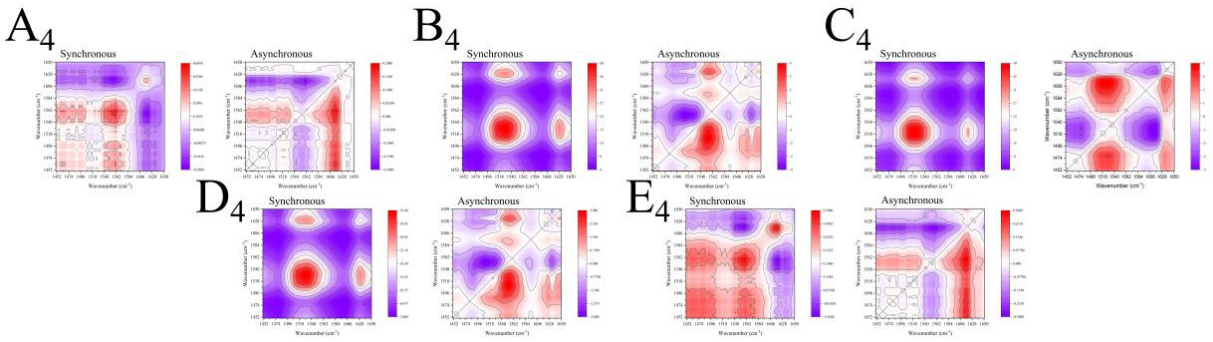

Fig. 3 Effect of OPS on the 2D FTIR spectra (A_1-E_1) of SR-IR, 3D FTIR spectra (A_2-E_2) of SR-IR, before and after 2D FTIR (A_3-E_3) and 2D-COS (A_4-E_4) of PWP-OPS with different OPS levels (0 - 0.75%, w/v)

Note: In order to help analyze SR-IR, the before and after 2D FTIR image was separated from 2D FTIR.

3.9.2. 2D-COS analysis

The correlation characteristic of SR-IR could be evaluated by 2D-COS. 2D-COS has the advantages of high resolution and the ability to resolve overlapping peaks in complex systems. It can effectively identify structural changes under external disturbances, thereby revealing the interaction mechanism [77]. The 2D-COS correlation peaks were presented as diagonal and non-diagonal (Fig. 3A_4-E_4) [31,78]. In general, when the changes in chemical composition were more pronounced, the color was darker. The characteristic vibration regions of the secondary structure of proteins, such as the amide I band (approximately 1600–1700 cm^{-1}, mainly including C=O stretching vibration, which can be further decomposed into conformations like α-helix and β-sheet) and the amide II band (approximately 1480–1580 cm^{-1}, mainly resulting from N-H bending and C-N stretching vibration), their dynamic changes can be analyzed through the cross-peak in the corresponding wave number range [79]. As shown in Fig. 3A_4 synchronization diagram, there were 5 autocorrelation peaks in the diagonal positions at 1460, 1488, 1516, 1560, and 1618 cm^{-1}, respectively. The peak at 1460 cm^{-1} might be related to the stretching vibration of the C-H bond of OPS, while the peaks at 1516, 1560, and 1618 cm^{-1} might be mainly affected by the bending vibration of the N-H bond and C-N bond of WPI. The asynchronous diagram was composed of cross peaks on two sides, reflecting the degree of correlation between absorption peaks. Positive cross peaks appeared at (1615 cm^{-1}, 1560 cm^{-1}), indicating that this group might have a synergistic effect with temperature perturbations. While a negative cross peak appeared at (1561 cm^{-1}, 1615 cm^{-1}), indicating an opposite response. A closer examination of the synchronous two-dimensional correlation spectra of the PWP-OPS sample in Figure 3B_4–E_4 revealed that the number of cross-peak intensities significantly increased within the range of 1600–1640 cm^{-1}. This region mainly corresponds to the signal of the β-sheet structure in the amide I band, indicating that the conformational vibration patterns of PWP-OPS changed more significantly during the temperature variation process [34].

3.10. Microstructure analysis

Cryo-SEM analysis revealed the microstructure of the PWP-OPS hydrogels. The PWP hydrogels exhibited a disordered network (Fig. 4A), potentially due to the formation of water channels during the thermally-induced gelation process, which disrupted the protein structure and compromised the integrity of

the hydrogel network and protein function [71,80]. The addition of 0.1% OPS to the hydrogel resulted in a more elongated and ordered microstructure. As the OPS concentration increased, the three-dimensional network structure became more compact and structured (Fig. 4B-E). This is attributed to the water absorption properties of OPS, which possesses a loose network structure that enables greater interaction between hydrophilic groups and water molecules [22]. During hydrogel formation, OPS could reduce water outflow, thereby protecting the hydrogel structure and leading to a more distinct and regular three-dimensional network with fewer pores, which enhanced the water-holding capacity of the hydrogel [71]. Previous studies have also shown that OPS can improve the network structure of PWP through multiple interactions, promoting protein aggregation, exposing more binding sites, facilitating OPS binding, and forming a stable three-dimensional network structure [64,81].

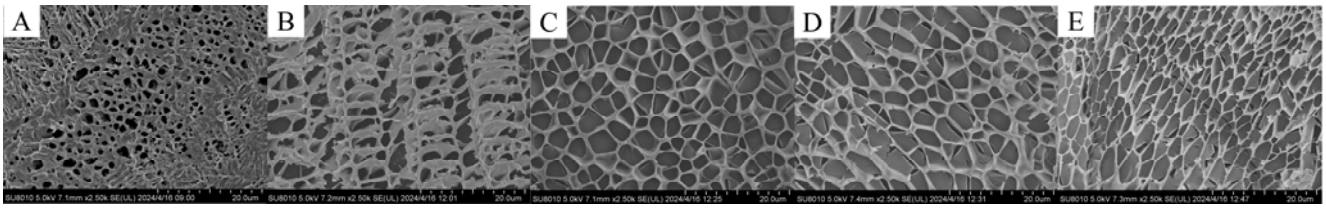

Fig. 4 Cryo-SEM (A-E) images (×2500) of PWP-OPS with different OPS levels (0-0.75%, w/v)

3.11. Molecular docking

Molecular docking analysis suggested a potential interaction between ovine polysaccharide (OPS) and β-lactoglobulin, with a predicted binding energy of -6.7 kcal/mol, indicative of a spontaneous association [82,83]. The complex formation was characterized by the establishment of multiple hydrogen bond interactions between the two biomolecules (Fig. 5A). Structural analysis revealed that OPS bound to protein-binding cavities of β-lactoglobulin, facilitating the establishment of various non-covalent interactions, thereby stabilizing the OPS-β-lactoglobulin complex.

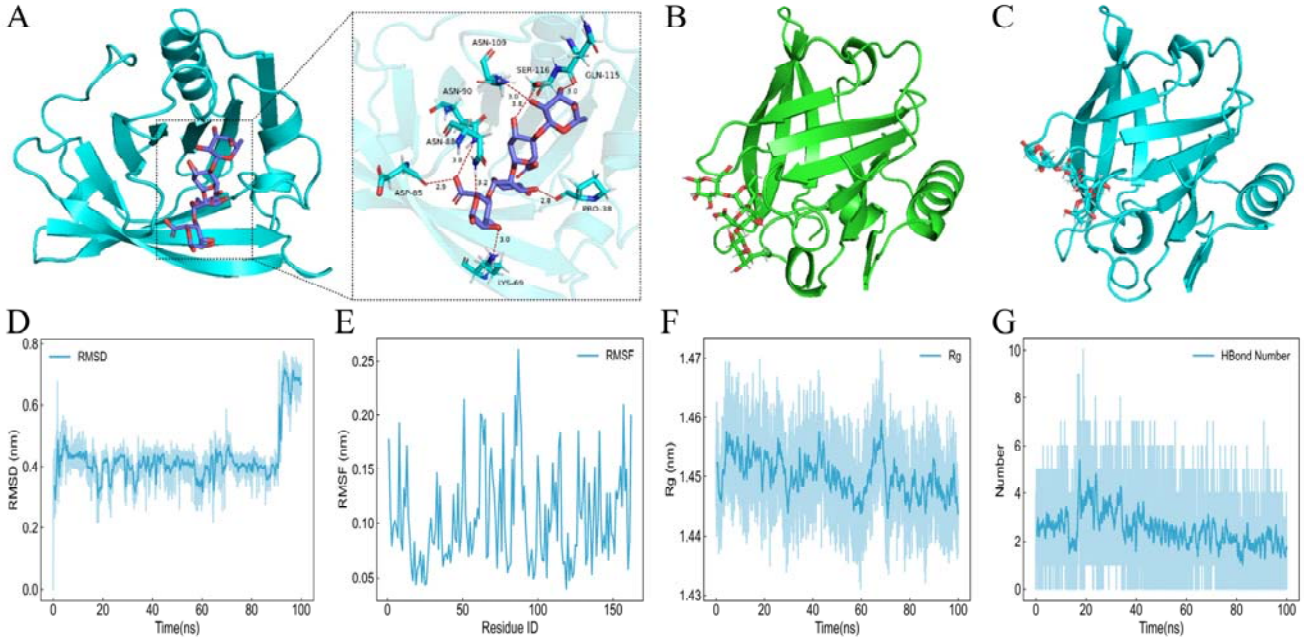

Fig. 5 Simulation of molecular docking (A), molecular dynamics RMSD (B), RMSF (C), Rg (D), Hydrogen bond number (E), Render snapshot of β-Lactoglobulin-OPS complex at 0ns (F) and Render snapshot of β-Lactoglobulin-OPS complex at 100ns (G) of β-Lactoglobulin-OPS

3.12. Molecular dynamics analysis

3.12.1. Root mean square deviation (RMSD) analysis

RMSD curves of OPS exhibited a notable increase during the initial dynamic phase (Fig. 5B), likely due to the presence of a random coil in the binding cavity. This coil gradually shifted from its original position under the influence of the surrounding environment and OPS, enlarging the β-lactoglobulin binding cavity. Subsequently, OPS remained stably bound within the cavity for up to 85 ns. The fluctuations in the RMSD curve during this period might be attributed to OPS's inherent flexibility and high rotational freedom. Beyond 85 ns, the introduction of OPS affected the β-lactoglobulin binding cavity, causing the β-folded region to deviate from its original position, leading to a new protein folding. This resulted in a further expansion of the OPS binding cavity. The relative size of the OPS binding cavity could be inferred as OPS interacted with the protein, enlarging the cavity through hydrogen bonding and van der Waals forces. Following the expansion of the β-lactoglobulin cavity, the OPS maintained stability throughout the simulation, indicating a significant impact of the tight OPS-β-lactoglobulin binding on the protein's structure. This suggested that a stable interaction between OPS and the protein was established during the 100 ns molecular dynamics simulation.

3.12.2. Root mean square fluctuation (RMSF) analysis

The overall root-mean-square fluctuation (RMSF) of β-lactoglobulin remained low throughout the simulation (Fig. 5C). The elevated RMSF observed at the N- and C-termini could be attributed to their peripheral location, which conferred greater flexibility due to reduced constraints from other protein domains. The RMSD analysis revealed an expansion of the OPS-binding cavity following OPS binding, driven by steric hindrance and hydrogen bond interactions. This process was accompanied by random twisting of the binding cavity and further movement of the β-fold segment, resulting in an enlarged binding cavity. Consequently, some flexible residues exhibited increased fluctuations, leading to higher RMSF values.

3.12.3. Radius of gyration (Rg) analysis

The β-lactoglobulin Rg curve remained largely unchanged throughout the simulation, indicating the protein's overall stability (Fig. 5D). Around 60 ns, the curve exhibited sharp fluctuations due to strong interactions between OPS and β-lactoglobulin. The introduction of OPS, along with steric hindrance and hydrogen bonding, enlarged the binding cavity and promoted β-lactoglobulin's β-folding tendency. During the simulation, small and medium-sized molecules penetrated deeper into the expanding binding cavity, interacting with the side chains of β-lactoglobulin surface residues. This interaction altered the side chain's tightness relative to the main chain, causing fluctuations in the Rg curve. After 80 ns, the Rg curve stabilized as the protein reached equilibrium, and the flexible residues in the binding cavity showed reduced movement. Consequently, the binding cavity stabilized, and OPS binding with the protein became more intimate, leading to further convergence of the RMSD curve. The β-lactoglobulin-OPS complex remained stable beyond 80 ns, with no significant changes observed.

3.12.4. Hydrogen bond number analysis

Throughout the simulation, the number of hydrogen bonds between OPS and β-lactoglobulin remained relatively stable, fluctuating within a specific range (Fig. 5E). The dynamic interactions between residues and OPS induced significant flexibility in OPS, leading to the formation and dissolution of hydrogen bonds with the protein-binding cavities. This resulted in fluctuations in the hydrogen bond number over time. When OPS transitioned into a new binding cavity, β-lactoglobulin tended to stabilize. Due to OPS's high rotational flexibility, it continuously adjusted its conformation in response to environmental influences and interactions with binding cavity residues. Despite fluctuations in the hydrogen bond count, it consistently ranged from 1 to 4, indicating a stable binding interaction between OPS and the protein.

3.12.5. Initial/final state comparison analysis

The initial (0 ns) and final (100 ns) states of the β-lactoglobulin-OPS complex were analyzed using PyMOL to elucidate the structural changes occurring during the 100 ns molecular dynamics simulation (Fig. 5F and Fig. 5G). Comparison of the two structures revealed a shift in the position of OPS relative to the protein over the course of the simulation. The binding cavity originally occupied by the ligand moved closer to the center of the protein, accompanied by an enlargement of the cavity. Concurrently, the β-sheets and random coil regions of β-lactoglobulin reoriented within the binding cavity, gradually moving apart and further expanding the binding site. These structural rearrangements were consistent with the observed fluctuations in the RMSF curve and the convergence of the radius of gyration (Rg) over the simulation time.

3.13. PH value of yogurt

The pH dynamics of yogurt fermentation are critical for product quality. Qin et al. [84] demonstrated that yogurts formulated with PWP-OPS hydrogels exhibited a slower decrease in pH compared to control samples during the fermentation process (Fig. 6A). The initial rapid decline (0-200 min) corresponded to the exponential growth phase of the starter cultures, while the subsequent deceleration and stabilization (200-360 min) occurred as the pH approached the proteins' isoelectric point and substrate became limited. This was because the PWP-OPS hydrogel itself possesses an enhanced buffering capacity near the protein's isoelectric point, thus requiring more lactic acid to be produced to achieve the same pH drop [32]. Therefore, the addition of PWP-OPS hydrogel could reduce probiotic activity damage caused by rapid pH changes [32]. These findings suggested that the incorporation of PWP-OPS hydrogels could modulate the pH profile of yogurt during fermentation, potentially optimizing product quality.

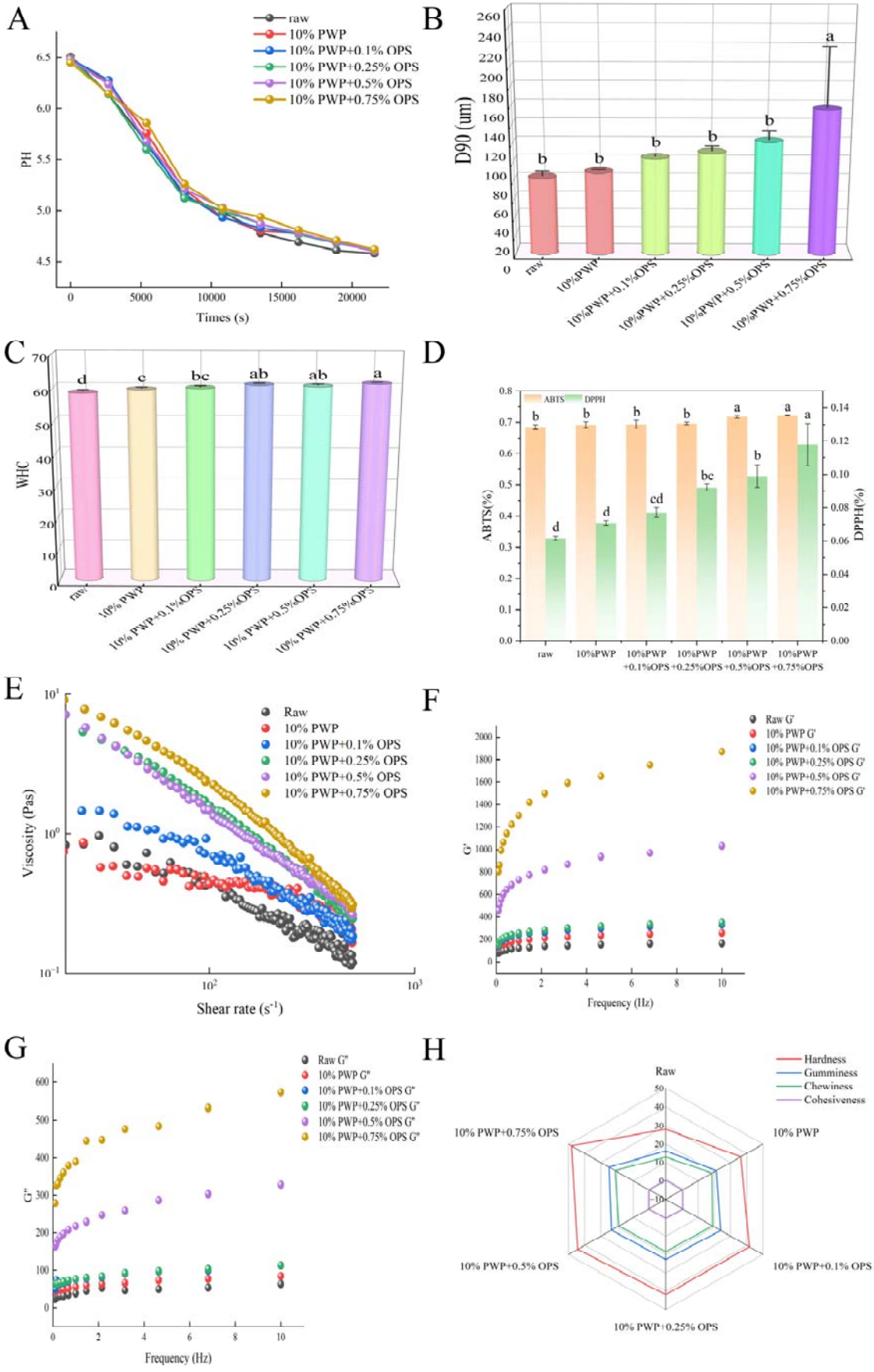

Fig. 6 The pH value (A), particle size (B), WHC (C), DPPT and ABTS (D), apparent viscosity (E), G′ (F), G″ (G), texture (H) of yogurt using PWP-OPS as a food additive

Note: The six yogurts were yogurts without PWP-OPS hydrogel, yogurts with 1% hydrogels containing 10% PWP, and different levels of OPS (0-0.75%, w/v).

3.14. Size of yogurt

The particle size distribution is a critical parameter for evaluating product stability and sensory quality, as it directly influences the microstructure and, consequently, the texture and mouthfeel of the product [54]. This characteristic is also closely linked to the sensory quality of the product. Particle size changes are primarily driven by two factors: the concentration and structural integrity of casein micelles, and the spatial arrangement of dissolved macromolecular substances in the aqueous phase [27,32]. The D90 value, which represents the particle diameter at the 90% cumulative distribution point, is commonly used to characterize the particle size distribution [32]. As the OPS content in the PWP-OPS hydrogel increased, the D90 value of the yogurt samples also rose, ranging from 83.8 μm to 157 μm (Fig. 6B). First, the hydrogel particles did not merely exist as inert fillers; rather, they actively participated in the gel network. The exposed functional groups on the PWP-OPS complex could act as additional cross-linking sites, bridging adjacent casein micelles and fat droplets to form larger, more cohesive clusters [85–87]. Secondly, this hydrogel possessed a pre-formed, dense three-dimensional network structure and interacted favorably with components such as casein in yogurt. Consequently, it could effectively fill the voids within the natural protein matrix and bridge the gaps between casein aggregates [88], thereby forming a more robust, continuous, and compact protein network, which was beneficial for the overall structure of the yogurt.

3.15. WHC of yogurt

WHC is a crucial indicator for evaluating yogurt quality, as it directly impacts product yield, texture, and sensory perception [42]. The addition of PWP-OPS hydrogels resulted in a significant and concentration-dependent improvement in WHC, with values increasing from 58.69% (control) to 61.51% (10% PWP+0.75% OPS) (Fig. 6C). Previous studies have demonstrated that the dry matter content and natural protein concentration significantly influence the properties of different proteins and the WHC in yogurt [89,90]. Given the consistent total solid content across all groups, this enhancement was unequivocally attributed to the unique functional role of the PWP-OPS complex within the protein matrix. PWP-OPS hydrogel actively integrated into the casein network, forming a composite gel through synergistic interactions. The polysaccharide chains of OPS enhanced cross-linking with casein, while the pre-formed hydrogel particles acted as structural reinforcements. This collaborative action led to the formation of a more uniform, fine-stranded, and continuous network, characterized by smaller and more numerous pores. This refined microstructure exerted stronger capillary forces and provided a greater surface area for water entrapment, effectively immobilizing a larger amount of free water and minimizing syneresis [91–93]. Consequently, the improved WHC provided a direct explanation for the superior textural properties.

3.16. Antioxidant property analysis

The free radical scavenging capacity of the yogurt, as assessed by DPPH and ABTS assays, exhibited a significant positive correlation with the OPS content in the incorporated PWP-OPS hydrogel (Fig. 6D). This enhancement in antioxidant activity could be attributed to two synergistic mechanisms. Primarily, it stems from the intrinsic radical-scavenging ability of OPS, which is rich in antioxidant functional groups such as

hydroxyl and carboxyl groups [94]. Secondly, the unique physical structure of the PWP-OPS hydrogel plays a critical role. As extensively characterized in Sections 3.3 and 3.10, the hydrogel formed a dense, three-dimensional network. This network could act as a physical barrier, compartmentalizing and reducing the mobility of pro-oxidants within the yogurt matrix. More importantly, it could effectively encapsulate [95] and protect oxidation-sensitive components like casein and unsaturated lipids, thereby shielding them from free radical attack and slowing down the propagation of oxidative chain reactions. Consequently, the incorporation of PWP-OPS not only directly quenched free radicals but also fortified the yogurt's inherent oxidative stability, a property that is crucial for preserving sensory quality and extending the product's shelf life.

3.17. The rheological properties of yogurt

The rheological properties of yogurt demonstrate its gel-like characteristics. The G' was observed to be higher than the G" (Fig. 6E-F), indicating the predominance of elastic over viscous deformation [96]. The addition of PWP-OPS to goat yogurt resulted in an increase in both G' and G", suggesting stronger molecular interactions between the yogurt components and the PWP-OPS [97]. The thermally denatured whey proteins in PWP-OPS can form hydrogen bonds, hydrophobic interactions, and disulfide bonds with the casein, leading to the formation of aggregates that stabilize the yogurt network structure [98]. Simultaneously, the OPS component, through its polyhydroxy structure, formed extensive hydrogen bonds with both PWP and casein, effectively stitching the protein particles into a more cohesive and continuous matrix. This synergistic interaction transformed the PWP-OPS hydrogel from a mere inclusion into a structural backbone that percolated throughout the system [99]. A similar enhancement of G' and G" has been reported for yogurt containing whey protein aggregates [54,100].

The apparent viscosity of yogurt samples exhibited a shear-thinning behavior, decreasing with increasing shear rate. However, the addition of PWP-OPS resulted in an increase in viscosity (Fig. 6G). This phenomenon might be attributed to the formation of denser and more viscous droplets by PWP-OPS, which could influence the uniformity of yogurt aggregates. Alternatively, the binding of PWP-OPS to casein in the yogurt matrix might restrict water mobility, thereby promoting an increase in viscosity [101]. These findings suggested that PWP-OPS could serve as an effective thickening agent for yogurt formulations.

3.18. Texture analysis of yogurt

The textural properties of yogurt are a critical indicator of its quality [42]. The addition of PWP-OPS was found to increase the hardness, gumminess, and chewiness of yogurt, while decreasing its cohesiveness (Fig. 6H). This phenomenon could be attributed to the enhanced interaction between PWP-OPS and casein, which promoted the aggregation of casein. Consequently, the density of the protein matrix was increased, resulting in a firmer and thicker yogurt texture [97]. Regarding cohesiveness, the values ranged from 0.3 to 0.7, with a downward trend observed as the OPS content increased, indicating improved smoothness [32]. The optimal textural properties were observed in the 10% PWP-0.75% OPS group.

3.19. Sensory analysis

3.19.1. Electronic nose analysis

The electronic nose detects volatile organic compounds using a sensor array that mimics the human sense of smell [102]. Aromatic values represent the concentration of these volatile substances (Fig. 7A1). As illustrated, the overall trend showed an increase in aromatic, likely due to PWP-OPS enhancing lactic acid bacteria metabolism during fermentation, thereby producing more esters and aldehydes and boosting aromatic qualities. Broadrange values reflect the cumulative signals of various volatile compounds, suggesting that PWP-OPS might stabilize these substances by forming a denser gel network with casein, thus reducing volatilization. Trends in hydrogen, arom-aliph, broad-methane, and methane-aliph decreased, indicating that PWP-OPS could extend shelf life. Data revealed that increasing OPS content with PWP-OPS addition inhibited the oxidative chain reaction of fats, reducing byproducts like malondialdehyde and maintaining a stable proportion. Moreover, higher OPS content appeared to inhibit hydrogen-metabolizing enzymes in methanogens, proteases, or lactic acid bacteria, thereby reducing the production of sulfur-containing amino acids and hydrogen. The sulfur-organic data showed minimal change, suggesting no spoilage or unpleasant odor when comparing the initial and subsequent yogurt samples. In contrast, the broad-alcohol data initially rose and then declined, possibly due to the preferential utilization of OPS in PWP-OPS by lactic acid bacteria, which might reduce the production of secondary metabolites like ethanol. Then, principal component analysis (PCA) was performed on yogurt samples with varying PWP-OPS concentrations. PC1 (the first principal component) accounted for 53.9% of the variance, which meant that the distribution of samples from left to right in the graph represented their most significant odor differences (Fig. 7B1). Notably, the control group (without PWP-OPS) was distinctly separated in a separate region, indicating that the incorporation of PWP-OPS indeed induced significant differences in the yogurt samples. The PCA data clearly demonstrated the significant positive effect of PWP-OPS, particularly its OPS component, on the overall olfactory profile of goat milk yogurt. This enhancement was visually evidenced by the systematic migration of sample points toward the positive direction of PC1, a region characterized by high aroma and low off-odor. Concurrently, the concurrent distancing of these samples from the negative PC1 axis—associated with spoilage- and oxidation-related volatiles—provided compelling evidence for the efficacy of PWP-OPS in extending product shelf-life by suppressing the generation of these undesirable compounds.

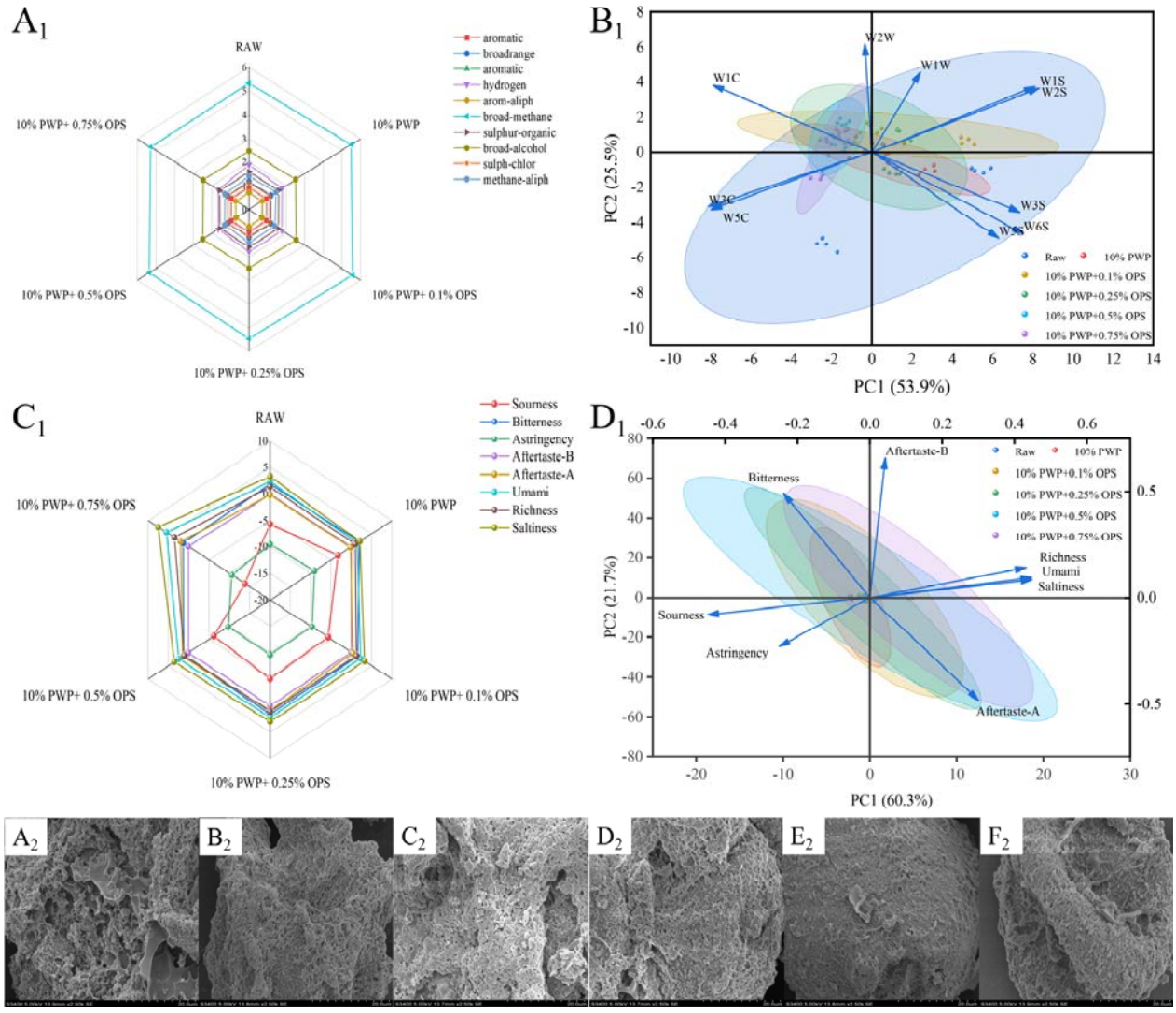

Fig. 7 The radar map of electronic nose (A_1), the PCA picture of electronic nose (B_1) the radar map of electronic tongue (C_1), the PCA picture of electronic tongue (D_1) and SEM (A_2-F_2) images (×2500) of yogurt using PWP-OPS as a food additive

Note: The six yogurts were yogurts without PWP-OPS hydrogel, yogurts with 1% hydrogels containing 10% PWP, and different levels of OPS (0 - 0.75%, w/v)

3.19.2. Electronic tongue

Electronic tongues are frequently employed to assess the taste profile of foods [103]. Analysis of electronic tongue data across eight dimensions revealed that increasing OPS in PWP-OPS hydrogel yogurt reduced acidity, bitterness, and astringency, while enhancing the responses of the other five sensors (Fig. 7C_1). This suggested that augmenting OPS content in PWP-OPS hydrogel during yogurt fermentation could retard acidification. Additionally, the hydrogel might inhibit yogurt spoilage during storage, preserving quality, as corroborated by electronic nose and pH measurements. The inclusion of PWP-OPS also improved aftertaste perception, likely due to the hydrogel's tight binding with casein, which delayed aftertaste detection [92,104]. Furthermore, umami and richness were moderately enhanced, implying that interactions between PWP-OPS hydrogel and yogurt proteins generate additional flavor carriers [105]. As shown in Fig. 7D_1, the first two principal components (PC1: 60.3% and PC2: 21.7%) collectively accounted for 82.0% of the total

variance. PC1, explaining 60.3% of the variance, served as the primary dimension differentiating the taste profiles of the samples. The loading structure of PC1 revealed clear sensory implications: its positive direction was strongly correlated with favorable attributes such as richness and umami, while the negative direction was closely associated with undesirable tastes, including bitterness, sourness, and astringency. This suggested that PC1 could be interpreted as a "palatability gradient," where higher scores along PC1 corresponded to improved overall taste perception. The distribution of samples in the PCA score plot demonstrated a clear and significant trend: with increasing OPS content in PWP-OPS, the sample points systematically shifted from the left region (Raw and 10% PWP) towards the positive direction of PC1, ultimately clustering in the right section of the plot. This spatial pattern confirmed that the addition of PWP-OPS effectively reduced negative tastes and synergistically enhanced positive flavors. The systematic migration along the PC1 axis strongly demonstrated, from a multivariate statistical perspective, that increasing the OPS content in the PWP-OPS hydrogel drove a fundamental shift in the overall taste profile of goat milk yogurt, transitioning from a profile dominated by bitterness, sourness, and astringency to one characterized by richness and umami.

3.20. Microstructure of yogurt using PWP-OPS hydrogels as a food additive

SEM provided direct visual evidence of the microstructural evolution in yogurt induced by the PWP-OPS hydrogel (Fig. 7A_2-F_2). The control yogurt exhibited a coarse, discontinuous network with large, irregular pores and a dispersed protein distribution. In stark contrast, the incorporation of PWP-OPS elicited a profound transformation, resulting in a progressively denser, more continuous, and uniform microstructure with diminishing pore size as the OPS content increased. This striking visual evidence served as the microstructural corroboration of the mechanisms proposed throughout this study. The formation of this refined architecture could be definitively attributed to the PWP-OPS complex acting as an integral structural unit and molecular bridge within the casein matrix [2]. As established by our molecular and spectroscopic analyses, the interactions—including hydrogen bonding, hydrophobic forces, and electrostatic interactions—enabled the hydrogel to seamlessly incorporate into and reinforce the native protein network [26]. This integration filled the voids observed in the control sample and promoted extensive cross-linking, effectively building bridges between casein clusters [106]. Then the yogurt formed a highly ordered network structure [107]. The resultant, highly interconnected network was fundamentally responsible for the enhanced macroscopic properties: the finer pore structure directly explained the superior water-holding capacity by exerting stronger capillary forces, while the increased structural continuity and density provided the physical basis for the improved rheological modulus and textural firmness.

3.21. Correlation analysis

The correlation scatter plots help analyze the relationship between structures and physicochemical properties [51]. For the PWP-OPS hydrogel itself (Fig. 8A), the strong positive correlation between 2D intrinsic fluorescence and surface hydrophobicity indicated a concerted change in the protein's tertiary structure. This was a direct statistical validation of the conformational changes observed in Sections 3.6 and 3.7, where the addition of OPS led to the burial of aromatic amino acids and a reduction in hydrophobic

surface exposure, driven by the formation of a more compact structure. The positive correlation of DSC (thermal stability) with particle size and free sulfhydryl content revealed that the OPS-induced aggregation (Section 3.1) created a more cross-linked network. This network not only had larger hydrodynamic dimensions but also possessed enhanced thermal stability. In summary, the structure of proteins (secondary and tertiary structure) was affected by surface hydrophobicity, hydrogen bonding, and intermolecular interactions (Fig. 8C).

The correlation matrix for yogurt (Fig. 8B) powerfully encapsulated how the PWP-OPS hydrogel transformed the product's physical properties. The strong positive cluster among apparent viscosity, particle size, water-holding capacity (WHC), and texture parameters (hardness, chewiness, gumminess) demonstrated that the microstructural consolidation observed via SEM (Section 3.20) had direct and simultaneous macroscopic consequences. The hydrogel promoted casein cross-linking and aggregation (increased particle size), which constructed a denser network (increased hardness) that effectively immobilized water (increased WHC) and resisted flow (increased apparent viscosity). The negative correlation between this cluster and cohesiveness was particularly insightful; it indicated that while the gel became firmer and more water-bound, it also became less prone to internal fracturing, resulting in a smoother and more homogeneous body, which was a desirable sensory attribute. The linkage of pH to this cluster further supported the mechanism proposed in Section 3.13, whereby the modulated acidification rate, influenced by the hydrogel's buffering capacity and micro-diffusion barriers, promoted the formation of this superior gel network.

In conclusion, the molecular-level interactions between OPS and PWP (hydrogen bonding, hydrophobic forces) induced a structural compaction and aggregation, which was manifested as enhanced thermal and rheological stability in the hydrogel. When incorporated into yogurt, this composite structure acted as a versatile functional ingredient that systematically enhanced the product's key quality attributes—texture, stability, and water retention-by fundamentally restructuring the casein matrix into a more unified and robust network.

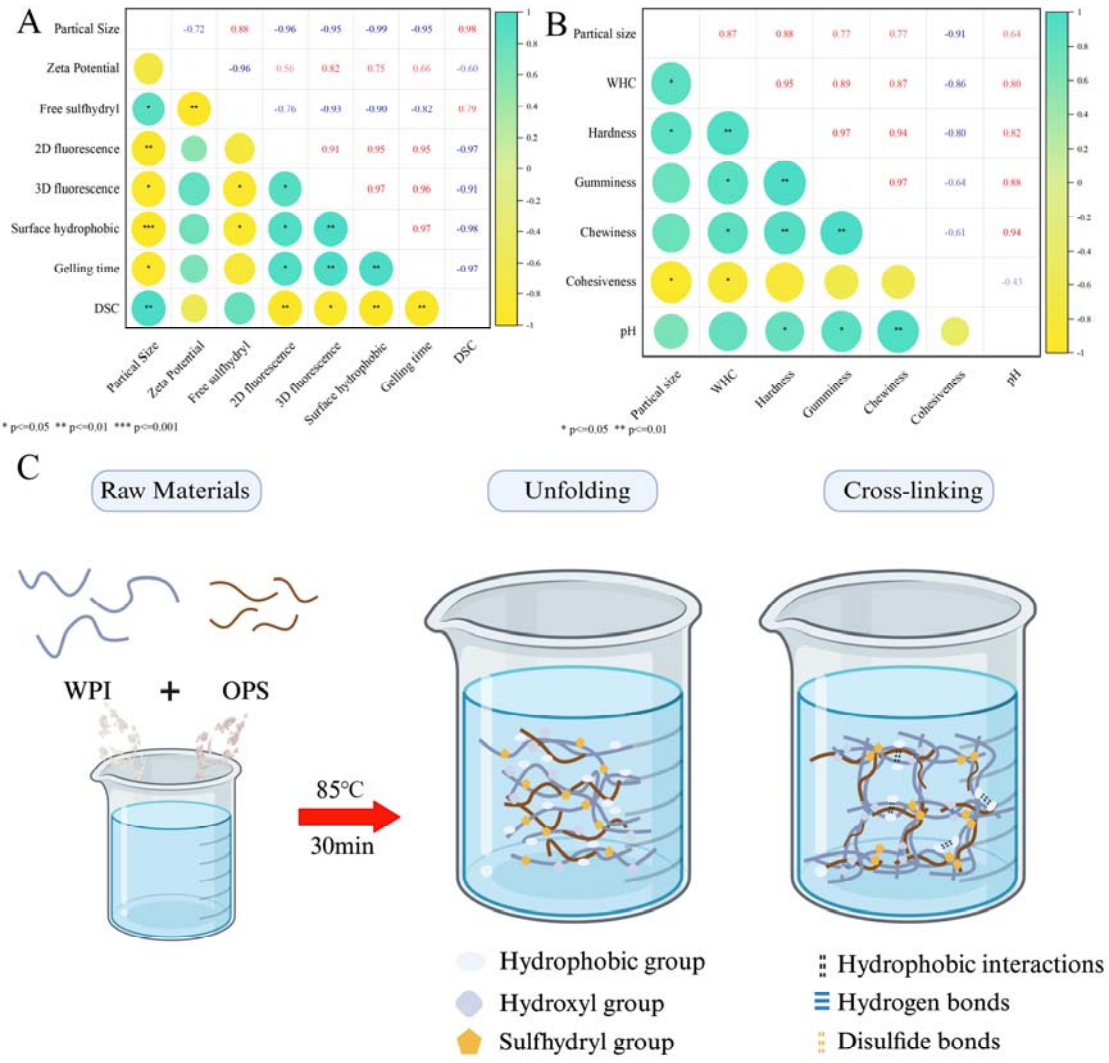

Fig. 8 The correlation of PWP-OPS (A), yogurt using PWP-OPS as a food additive (B) and the bonding mechanism diagram of PWP-OPS (C)

Note: The six yogurts were yogurts without PWP-OPS hydrogel, yogurts with 1% hydrogels containing 10% PWP, and different levels of OPS (0-0.75%, w/v)

4. Conclusions

The interaction between polymerized whey protein (PWP) and okra polysaccharide (OPS) was investigated using advanced analytical techniques, including SR-IR, molecular docking, and molecular dynamics simulations. These analyses revealed that PWP and OPS could form a complex through hydrogen bonding, electrostatic interactions, and hydrophobic interactions. Compared to PWP alone, the PWP-OPS hydrogel exhibited a denser and more stable three-dimensional network structure, as well as improved antioxidant properties and stability. Furthermore, the potential application of the PWP-OPS complex as a yogurt thickener was evaluated. Results demonstrated that the incorporation of 1% PWP-OPS, containing 0.75% OPS and 10% PWP, could significantly enhance the texture and sensory characteristics of yogurt. The superior gelation and functional properties of the PWP-OPS hydrogel suggest its significant potential for applications beyond yogurt, such as in plant-based dairy alternatives, processed meats, and edible coatings, which represents a promising direction for future research.

Declaration of Competing of Interest

The authors declare that they have no known competing financial interests or personal relationships that could have appeared to influence the work reported in this paper.

References

[1] M. Albenzio, A. Campanozzi, M. D'Apolito, A. Santillo, M.P. Mantovani, A. Sevi, Differences in protein fraction from goat and cow milk and their role on cytokine production in children with cow's milk protein allergy, Small Ruminant Research 105 (2012) 202–205. https://doi.org/10.1016/j.smallrumres.2012.02.018.

[2] M. Hovjecki, M. Radovanovic, Z. Miloradovic, I. Barukcic Jurina, M. Mirkovic, I. Sredovic Ignjatovic, J. Miocinovic, Fortification of goat milk yogurt with goat whey protein concentrate – Effect on rheological, textural, sensory and microstructural properties, Food Bioscience 56 (2023) 103393. https://doi.org/10.1016/j.fbio.2023.103393.

[3] R. Kapila, P.K. Kavadi, S. Kapila, Comparative evaluation of allergic sensitization to milk proteins of cow, buffalo and goat, Small Ruminant Research 112 (2013) 191–198. https://doi.org/10.1016/j.smallrumres.2012.11.028.

[4] G.A. Nayik, Y.D. Jagdale, S.A. Gaikwad, A.N. Devkatte, A.H. Dar, M.J. Ansari, Nutritional Profile, Processing and Potential Products: A Comparative Review of Goat Milk, Dairy 3 (2022) 622–647. https://doi.org/10.3390/dairy3030044.

[5] S. Verruck, A. Dantas, E.S. Prudencio, Functionality of the components from goat's milk, recent advances for functional dairy products development and its implications on human health, Journal of Functional Foods 52 (2019) 243–257. https://doi.org/10.1016/j.jff.2018.11.017.

[6] J. Domagała, Instrumental Texture, Syneresis and Microstructure of Yoghurts Prepared from Goat, Cow and Sheep Milk, International Journal of Food Properties 12 (2009) 605–615. https://doi.org/10.1080/10942910801992934.

[7] J. Miocinovic, Z. Miloradovic, M. Josipovic, A. Nedeljkovic, M. Radovanovic, P. Pudja, Rheological and textural properties of goat and cow milk set type yoghurts, International Dairy Journal 58 (2016) 43–45. https://doi.org/10.1016/j.idairyj.2015.11.006.

[8] H.T.H. Nguyen, S. Afsar, L. Day, Differences in the microstructure and rheological properties of low-fat yoghurts from goat, sheep and cow milk, Food Research International 108 (2018) 423–429. https://doi.org/10.1016/j.foodres.2018.03.040.

[9] P. Caboni, A. Murgia, A. Porcu, C. Manis, I. Ibba, M. Contu, P. Scano, A metabolomics comparison between sheep's and goat's milk, Food Research International 119 (2019) 869–875. https://doi.org/10.1016/j.foodres.2018.10.071.

[10] K. Xu, M. Guo, J. Du, Z. Zhang, Okra polysaccharide: Effect on the texture and microstructure of set yoghurt as a new natural stabilizer, International Journal of Biological Macromolecules 133 (2019) 117–126. https://doi.org/10.1016/j.ijbiomac.2019.04.035.

[11] W. Wang, M. Shen, L. Jiang, Q. Song, S. Liu, J. Xie, Influence of Mesona blumes polysaccharide on the gel properties and microstructure of acid-induced soy protein isolate gels, Food Chemistry 313 (2020) 126125. https://doi.org/10.1016/j.foodchem.2019.126125.

[12] Q. Ban, Z. Liu, X. Zhang, B. Song, Y. Jiang, J. Cheng, Improvement of non-fat yogurt gel syneresis by heat-unfolded whey protein isolate/mogrosides complexes: Effect on the structural characterization through simultaneous rheological and FTIR techniques, Food Hydrocolloids 144 (2023) 109025. https://doi.org/10.1016/j.foodhyd.2023.109025.

[13] X. Liu, J.R. Powers, B.G. Swanson, H.H. Hill, S. Clark, Modification of whey protein concentrate hydrophobicity by high hydrostatic pressure, Innovative Food Science & Emerging Technologies 6 (2005) 310–317. https://doi.org/10.1016/j.ifset.2005.03.006.

[14] M.C. Devries, S.M. Phillips, Supplemental Protein in Support of Muscle Mass and Health: Advantage Whey, Journal of Food Science 80 (2015). https://doi.org/10.1111/1750-3841.12802.

[15] S. Gunasekaran, S. Ko, L. Xiao, Use of whey proteins for encapsulation and controlled delivery applications, Journal of Food Engineering 83 (2007) 31–40. https://doi.org/10.1016/j.jfoodeng.2006.11.001.

[16] A. Yiğit, P. Bielska, D. Cais-Sokolińska, G. Samur, Whey proteins as a functional food: Health effects, functional properties, and applications in food, Journal of the American Nutrition Association 42 (2023) 758–768. https://doi.org/10.1080/27697061.2023.2169208.

[17] H. Xiang, Z. Jiang, W. Tao, S. Lv, Y. Li, J. Peng, C. Wang, H. Ju, X. Sun, C. Li, Insight into structural changes in heat-induced whey protein-fucoidan hydrogel by SR-IR and molecular docking techniques, Food Research International 197 (2024) 115222. https://doi.org/10.1016/j.foodres.2024.115222.

[18] X. Zhang, X. Sun, F. Gao, J. Wang, C. Wang, Systematical characterization of physiochemical and rheological properties of thermal-induced polymerized whey protein, J Sci Food Agric 99 (2019) 923–932. https://doi.org/10.1002/jsfa.9264.

[19] M. Nooshkam, M. Varidi, Whey protein isolate-low acyl gellan gum Maillard-based conjugates with tailored technological functionality and antioxidant activity, International Dairy Journal 109 (2020) 104783. https://doi.org/10.1016/j.idairyj.2020.104783.

[20] Z. He, T. Ma, W. Zhang, E. Su, F. Cao, M. Huang, Y. Wang, Heat-induced gel formation by whey protein isolate-Lycium barbarum polysaccharides at varying pHs, Food Hydrocolloids 115 (2021) 106607. https://doi.org/10.1016/j.foodhyd.2021.106607.

[21] B. Ozel, S.S. Uguz, M. Kilercioglu, L. Grunin, M.H. Oztop, Effect of different polysaccharides on swelling of composite whey protein hydrogels: A low field (LF) NMR relaxometry study, J Food Process Engineering 40 (2017) e12465. https://doi.org/10.1111/jfpe.12465.

[22] Z.-L. Chen, C. Wang, H. Ma, Y. Ma, J.-K. Yan, Physicochemical and functional characteristics of polysaccharides from okra extracted by using ultrasound at different frequencies, Food Chemistry 361 (2021) 130138. https://doi.org/10.1016/j.foodchem.2021.130138.

[23] X. Zhu, R. Xu, H. Wang, J. Chen, Z. Tu, Structural Properties, Bioactivities, and Applications of Polysaccharides from Okra [*Abelmoschus esculentus* (L.) Moench]: A Review, J. Agric. Food Chem. 68 (2020) 14091–14103. https://doi.org/10.1021/acs.jafc.0c04475.

[24] Z. Liao, Y. Li, L. Liao, Q. Shi, Y. Kong, J. Hu, Y. Cai, Structural characterization and anti-lipotoxicity effects of a pectin from okra (Abelmoschus esculentus (L.) Moench), International Journal of Biological Macromolecules 238 (2023) 124111. https://doi.org/10.1016/j.ijbiomac.2023.124111.

[25] M. Fatima, A. Rakha, A.B. Altemimi, F. Van Bocktaele, A.I. Khan, M. Ayyub, R.M. Aadil, Okra: Mucilage extraction, composition, applications, and potential health benefits, European Polymer Journal 215 (2024) 113193. https://doi.org/10.1016/j.eurpolymj.2024.113193.

[26] Y. Zhu, Z. Luo, H. Xiang, Y. Jiang, Z. Wang, Z. Jiang, X. Sun, X. Wang, Physicochemical properties and texture of polymerized whey protein-auric polysaccharide and its incorporation into goat milk yogurt, Food Research International 206 (2025) 115889. https://doi.org/10.1016/j.foodres.2025.115889.

[27] Z. Luo, Y. Zhu, H. Xiang, Z. Wang, X. Sun, Z. Guo, Characterization of heat-induced whey protein-Dendrobium officinale polysaccharide and its application in goat milk yogurt, International Journal of Biological Macromolecules 310 (2025) 143319. https://doi.org/10.1016/j.ijbiomac.2025.143319.

[28] Z. Zhou, H. Xiang, J. Cheng, Q. Ban, X. Sun, M. Guo, Effects of Panax notoginseng Saponins Encapsulated by Polymerized Whey Protein on the Rheological, Textural and Bitterness Characteristics of Yogurt, Foods 13 (2024) 486. https://doi.org/10.3390/foods13030486.

[29] H. Xiang, W. Tao, Y. Li, W. Mu, Y. Cheng, W. Shen, C. Wang, L. Guan, K. Wang, X. Sun, C. Li, Effects of induced electric field and high-pressure microjet sterilization on the physicochemical properties of milk, Food Science of Animal Products 2 (2024) 9240086. https://doi.org/10.26599/FSAP.2024.9240086.

[30] Y. Zhao, D. Wang, J. Xu, D. Tu, W. Zhuang, Y. Tian, Effect of polysaccharide concentration on heat-induced Tremella fuciformis polysaccharide-soy protein isolation gels: Gel properties and interactions, International Journal of Biological Macromolecules 262 (2024) 129782. https://doi.org/10.1016/j.ijbiomac.2024.129782.

[31] H. Xiang, W. Tao, Y. Su, Y. Jiang, Y. He, Y. Cheng, W. Mu, C. Wang, K. Wang, X. Chen, X. Sun, Effects of astragalus polysaccharide on the physicochemical properties of heat-induced whey protein gels by simultaneous rheology and Fourier transform infrared spectroscopy, Journal of Dairy Science 108 (2025) 4626–4637. https://doi.org/10.3168/jds.2025-26374.

[32] Z. Zhou, L. Zhang, T. Liu, G. Hu, H. Hu, T. Aziz, M. Zhang, J. Wu, J. Naseeb, Z. Yang, Z. Yang, T.H. Albekairi, Physicochemical properties of yoghurt supplemented with polymerized whey protein and inulin, LWT 210 (2024) 116888. https://doi.org/10.1016/j.lwt.2024.116888.

[33] Y. Meng, X. Zhao, Y. Jiang, Q. Ban, X. Wang, Effect of Maillard reaction conditions on the gelation and thermal stability of whey protein isolate/d-tagatose conjugates, Food Chemistry 405 (2023) 134928. https://doi.org/10.1016/j.foodchem.2022.134928.

[34] Z. Xing, J. Zhang, F. Lou, Z. Guo, L. Jiang, Q. Ban, Z. Wang, Reduction of soybean globulin antigen by soybean protein isolate/γ-aminobutyric acid complexes: Effect of the different concentrations of γ-aminobutyric acid on the protein modification, antigen levels, and foaming properties, Food Hydrocolloids 160 (2025) 110729. https://doi.org/10.1016/j.foodhyd.2024.110729.

[35] Y. Zhao, X. Wang, D. Li, H. Tang, D. Yu, L. Wang, L. Jiang, Effect of anionic polysaccharides on conformational changes and antioxidant properties of protein-polyphenol binary covalently-linked complexes, Process Biochemistry 89 (2020) 89–97. https://doi.org/10.1016/j.procbio.2019.10.021.

[36] S. Zhang, J. Hao, Q. Xie, X. Pi, Z. Peng, Y. Sun, J. Cheng, pH-induced physiochemical and structural changes of milk proteins mixtures and its effect on foaming behavior, International Journal of Biological Macromolecules 254 (2024) 127838. https://doi.org/10.1016/j.ijbiomac.2023.127838.

[37] Y. Zhang, Z. Zhang, Y. Fu, Y. Gao, W. Guo, R. Hu, X. Liu, Effects of different ph on properties of heat-induced Auricularia auricula-judae polysaccharide-whey protein isolate composite gels, Food Structure 36 (2023) 100317. https://doi.org/10.1016/j.foostr.2023.100317.

[38] S. Zhang, Y. Sun, Q. Xie, Y. Jiang, J. Cheng, Effect of different salts on the foaming properties of model protein systems for infant formula, Journal of Dairy Science 107 (2024) 2668–2680. https://doi.org/10.3168/jds.2023-24080.

[39] S. Liang, Y. Qin, Z. Bo, J. He, Q. Li, J. Sun, G. Zhang, C. Li, L. Liu, G. Huo, Molecular interaction mechanisms of Lactobacillus helveticus KLDS1.8701 on construction of yogurt gel network, transformation of milk protein conformation, and formation of characteristic flavor, Journal of Dairy Science (2025) S0022030225002899. https://doi.org/10.3168/jds.2025-26531.

[40] K. Zhang, H. Tang, M.S. Farid, F. Xiang, B. Li, Effect of Lactobacillus helveticus exopolysaccharides molecular weight on yogurt gel properties and its internal mechanism, International Journal of Biological Macromolecules 262 (2024) 130006. https://doi.org/10.1016/j.ijbiomac.2024.130006.

[41] Q. Ban, Z. Liu, C. Yu, X. Sun, Y. Jiang, J. Cheng, M. Guo, Physiochemical, rheological, microstructural, and antioxidant properties of yogurt using monk fruit extract as a sweetener, Journal of Dairy Science 103 (2020) 10006–10014. https://doi.org/10.3168/jds.2020-18703.

[42] T. Fang, X. Shen, J. Hou, M. Guo, Effects of polymerized whey protein prepared directly from cheese whey as fat replacer on physiochemical, texture, microstructure and sensory properties of low-fat set yogurt, LWT 115 (2019) 108268. https://doi.org/10.1016/j.lwt.2019.108268.

[43] X. Liu, X. Qin, Y. Wang, J. Zhong, Physicochemical properties and formation mechanism of whey protein isolate-sodium alginate complexes: Experimental and computational study, Food Hydrocolloids 131 (2022) 107786. https://doi.org/10.1016/j.foodhyd.2022.107786.

[44] R.A. Amos, M.A. Atmodjo, C. Huang, Z. Gao, A. Venkat, R. Taujale, N. Kannan, K.W. Moremen, D. Mohnen, Polymerization of the backbone of the pectic polysaccharide rhamnogalacturonan I, Nat. Plants 8 (2022) 1289–1303. https://doi.org/10.1038/s41477-022-01270-3.

[45] Y. Liu, X. Yang, J. Gan, S. Chen, Z.-X. Xiao, Y. Cao, CB-Dock2: improved protein–ligand blind docking by integrating cavity detection, docking and homologous template fitting, Nucleic Acids Research 50 (2022) W159–W164. https://doi.org/10.1093/nar/gkac394.

[46] Z. Cui, S. Wang, Y. Xu, Y. Liu, W. Wang, Potential of umami molecules against SARS-CoV-2 (Omicron) S-RBD/hACE2 interaction: an in-silico study, Journal of Future Foods 5 (2025) 283–294. https://doi.org/10.1016/j.jfutfo.2024.07.008.

[47] R. Salomon-Ferrer, D.A. Case, R.C. Walker, An overview of the Amber biomolecular simulation package, WIREs Comput Mol Sci 3 (2013) 198–210. https://doi.org/10.1002/wcms.1121.

[48] J.A. Maier, C. Martinez, K. Kasavajhala, L. Wickstrom, K.E. Hauser, C. Simmerling, ff14SB: Improving the Accuracy of Protein Side Chain and Backbone Parameters from ff99SB, J. Chem. Theory Comput. 11 (2015) 3696–3713. https://doi.org/10.1021/acs.jctc.5b00255.

[49] J. Wang, R.M. Wolf, J.W. Caldwell, P.A. Kollman, D.A. Case, Development and testing of a general amber force field, J Comput Chem 25 (2004) 1157–1174. https://doi.org/10.1002/jcc.20035.

[50] P. Mark, L. Nilsson, Structure and Dynamics of the TIP3P, SPC, and SPC/E Water Models at 298 K, J. Phys. Chem. A 105 (2001) 9954–9960. https://doi.org/10.1021/jp003020w.

[51] S. Zhang, Q. Xie, F. Wang, Y. Xie, J. Cheng, Q. Ban, Effects of mono- and divalent-ions and their strength on foaming properties of infant formula protein model system, Food Hydrocolloids 160 (2025) 110828. https://doi.org/10.1016/j.foodhyd.2024.110828.

[52] M. Liu, S. Shan, X. Gao, Y. Shi, W. Lu, The effect of sweet tea polysaccharide on the physicochemical and structural properties of whey protein isolate gels, International Journal of Biological Macromolecules 240 (2023) 124344. https://doi.org/10.1016/j.ijbiomac.2023.124344.

[53] Y. Zhang, Z. Wang, S. Yao, X. Lin, X. Zhang, X. Tan, L. Zhang, R. Xu, Y. Zhao, C. Zhao, F. Chu, W. Jing, X. Huang, P. Wang, Natural polysaccharide hydrogel with bioadhesion characters to synergistically enhance berberine's antibacterial effect by regulating the PTS system of Staphylococcus aureus, International Journal of Biological Macromolecules 281 (2024) 136605. https://doi.org/10.1016/j.ijbiomac.2024.136605.

[54] S. Lv, W. Tao, H. Xiang, Y. Zhang, A. Khan, S. Li, X. Yang, X. Sun, C. Li, Hydrogen-bond reinforced whey protein-polygonatum sibiricum polysaccharide composite hydrogel: Mechanistic insights from simultaneous rheology-FTIR and molecular docking for enhanced yogurt texture, Food Research International (2025) 117496. https://doi.org/10.1016/j.foodres.2025.117496.

[55] C.-E. Brunchi, M. Bercea, S. Morariu, M. Dascalu, Some properties of xanthan gum in aqueous solutions: effect of temperature and pH, J Polym Res 23 (2016) 123. https://doi.org/10.1007/s10965-016-1015-4.

[56] T. Gao, X. Wu, Y. Gao, F. Teng, Y. Li, Construction of emulsion gel based on the interaction of anionic polysaccharide and soy protein isolate: Focusing on structural, emulsification and functional properties, Food Chemistry: X 22 (2024) 101377. https://doi.org/10.1016/j.fochx.2024.101377.

[57] Y. Lin, Z. Wang, C. Shi, L. Han, Q. Yu, Potentially texture-modified food for dysphagia: Impact of Polygonatum sibiricum polysaccharide addition on gelling properties, microstructure and digestibility of bovine tendon collagen-cassava starch composite gels, Food Hydrocolloids 164 (2025) 111164. https://doi.org/10.1016/j.foodhyd.2025.111164.

[58] S. Wang, J. Yang, G. Shao, D. Qu, H. Zhao, L. Yang, L. Zhu, Y. He, H. Liu, D. Zhu, Soy protein isolated-soy hull polysaccharides stabilized O/W emulsion: Effect of polysaccharides concentration on the storage stability and interfacial rheological properties, Food Hydrocolloids 101 (2020) 105490. https://doi.org/10.1016/j.foodhyd.2019.105490.

[59] Y. Wu, C. Lei, J. Li, Y. Chen, H. Liang, Y. Li, B. Li, X. Luo, Y. Pei, S. Liu, Improvement of O/W emulsion performance by adjusting the interaction between gelatin and bacterial cellulose nanofibrils, Carbohydrate Polymers 276 (2022) 118806. https://doi.org/10.1016/j.carbpol.2021.118806.

[60] Y. Ma, H. Sun, S. Zhang, C. Yang, E. Musazade, H. Fan, T. Liu, Y. Zhang, Structural modification of whey protein isolate via electrostatic complexation with Tremella polysaccharides and its effect on emulsion stability at pH 4.5, International Journal of Biological Macromolecules 297 (2025) 139870. https://doi.org/10.1016/j.ijbiomac.2025.139870.

[61] Z. Liu, D. Lin, R. Shen, X. Yang, Bacterial cellulose nanofibers improved the emulsifying capacity of soy protein isolate as a stabilizer for pickering high internal-phase emulsions, Food Hydrocolloids 112 (2021) 106279. https://doi.org/10.1016/j.foodhyd.2020.106279.

[62] X.M. Sun, C.N. Wang, M.R. Guo, Interactions between whey protein or polymerized whey protein and soybean lecithin in model system, Journal of Dairy Science 101 (2018) 9680–9692. https://doi.org/10.3168/jds.2018-14998.

[63] M. Anvari, M. Tabarsa, R. Cao, S. You, H.S. Joyner (Melito), S. Behnam, M. Rezaei, Compositional characterization and rheological properties of an anionic gum from Alyssum homolocarpum seeds, Food Hydrocolloids 52 (2016) 766–773. https://doi.org/10.1016/j.foodhyd.2015.07.030.

[64] Z. Wang, J. Long, C. Zhang, Y. Hua, X. Li, Effect of polysaccharide on structures and gel properties of microgel particle reconstructed soybean protein isolate/polysaccharide complex emulsion gels as solid fat mimetic, Carbohydrate Polymers 347 (2025) 122759. https://doi.org/10.1016/j.carbpol.2024.122759.

[65] A.-C. Lee, Y.-H. Hong, Coacervate formation of α-lactalbumin–chitosan and β-lactoglobulin–chitosan complexes, Food Research International 42 (2009) 733–738. https://doi.org/10.1016/j.foodres.2009.02.022.

[66] Z. Xue, M. Zhang, J. Wang, S. Wang, S. Han, X. Huang, H. Liu, pH-regulated Tannic acid and soybean protein isolate adhesive for enhanced performance in plant-based meat analogues, Food Research International 185 (2024) 114289. https://doi.org/10.1016/j.foodres.2024.114289.

[67] A.F.M. Bora, K.J.E.-P. Kouame, X. Li, L. Liu, Y. Sun, Q. Ma, Y. Liu, Development, characterization and probiotic encapsulating ability of novel Momordica charantia bioactive polysaccharides/whey protein isolate composite gels, International Journal of Biological Macromolecules 225 (2023) 454–466. https://doi.org/10.1016/j.ijbiomac.2022.11.097.

[68] F. Alavi, S. Momen, Z. Emam-Djomeh, M. Salami, A.A. Moosavi-Movahedi, Radical cross-linked whey protein aggregates as building blocks of non-heated cold-set gels, Food Hydrocolloids 81 (2018) 429–441. https://doi.org/10.1016/j.foodhyd.2018.03.016.

[69] H. Xing, X. Liu, Y. Hu, K. Hu, J. Chen, Effect of Lycium barbarum polysaccharides on heat-induced gelation of soy protein isolate, Food Hydrocolloids 147 (2024) 109323. https://doi.org/10.1016/j.foodhyd.2023.109323.

[70] W. Li, Y. Guan, S. Chen, X. Du, B. Yan, Z. Wang, R. Ma, Y. Zhang, H. Huang, D. Li, W. Li, Effect of Lactobacillus pentosus fermentation on molecular structure and gel quality of peanut protein, Journal of Future Foods 5 (2025) 257–265. https://doi.org/10.1016/j.jfutfo.2024.07.005.

[71] W. Jiang, X. Yang, S. Yin, R. Li, S. Zhang, L. Li, Gelation behaviour of Auricularia polytricha polysaccharides-whey protein isolate, Journal of Food Engineering 377 (2024) 112079. https://doi.org/10.1016/j.jfoodeng.2024.112079.

[72] R. Li, N. Wang, C. Ma, J. Wang, J. Wang, X. Yang, Construction and formation mechanism of phase-change polysaccharide–protein composite emulsion gels: For simultaneous printing of food products with complex structures and fine patterns, Food Hydrocolloids 160 (2025) 110817. https://doi.org/10.1016/j.foodhyd.2024.110817.

[73] Q. Cheng, C. Liu, J. Zhao, J. Qin, Y. Wang, Hydroxyl radical-induced oxidation boosts the gelation of ginkgo seed protein in the presence of hyaluronic acid, International Journal of Biological Macromolecules 282 (2024) 136960. https://doi.org/10.1016/j.ijbiomac.2024.136960.

[74] M. Li, X. Hou, L. Lin, F. Jiang, D. Qiao, F. Xie, Legume protein/polysaccharide food hydrogels: Preparation methods, improvement strategies and applications, International Journal of Biological Macromolecules 243 (2023) 125217. https://doi.org/10.1016/j.ijbiomac.2023.125217.

[75] A. Khan, C. Wang, X. Sun, A. Killpartrick, M. Guo, Preparation and Characterization of Whey Protein Isolate–DIM Nanoparticles, IJMS 20 (2019) 3917. https://doi.org/10.3390/ijms20163917.

[76] M. Wang, Y. Fu, G. Chen, Y. Shi, X. Li, H. Zhang, Y. Shen, Fabrication and characterization of carboxymethyl chitosan and tea polyphenols coating on zein nanoparticles to encapsulate β-carotene by anti-solvent precipitation method, Food Hydrocolloids 77 (2018) 577–587. https://doi.org/10.1016/j.foodhyd.2017.10.036.

[77] W. Qi, Y. Xie, L. Sun, Z. Jiang, J. Cheng, Q. Ban, Investigating Hofmeister ions on rice starch gelatinization using simultaneous rheology and FTIR techniques combined with 2D correlation analysis, Food Hydrocolloids 165 (2025) 111265. https://doi.org/10.1016/j.foodhyd.2025.111265.

[78] I. Noda, Recent advancement in the field of two-dimensional correlation spectroscopy, Journal of Molecular Structure 883–884 (2008) 2–26. https://doi.org/10.1016/j.molstruc.2007.11.038.

[79] R. Zafar, Z. Arshad, N. Eun Choi, X. Li, J. Hur, Unravelling the complex adsorption behavior of extracellular polymeric substances onto pristine and UV-aged microplastics using two-dimensional correlation spectroscopy, Chemical Engineering Journal 470 (2023) 144031. https://doi.org/10.1016/j.cej.2023.144031.

[80] A.J. Gravelle, A.G. Marangoni, S. Barbut, Insight into the mechanism of myofibrillar protein gel stability: Influencing texture and microstructure using a model hydrophilic filler, Food Hydrocolloids 60 (2016) 415–424. https://doi.org/10.1016/j.foodhyd.2016.04.014.

[81] L. Sun, X. Ye, S. Liu, B. Safdar, J. Li, X. Liu, H. Li, Study on the mechanism of protein-polysaccharide complex high viscosity gel and its adhesion in plant meat substitute, International Journal of Biological Macromolecules 311 (2025) 143547. https://doi.org/10.1016/j.ijbiomac.2025.143547.

[82] H. Wang, H. Zhang, Q. Liu, X. Xia, Q. Chen, B. Kong, Exploration of interaction between porcine myofibrillar proteins and selected ketones by GC–MS, multiple spectroscopy, and molecular docking approaches, Food Research International 160 (2022) 111624. https://doi.org/10.1016/j.foodres.2022.111624.

[83] X. Wang, M. Li, T. Shi, A.R. Monto, L. Yuan, W. Jin, R. Gao, Enhancement of the gelling properties of Aristichthys nobilis: Insights into intermolecular interactions between okra polysaccharide and myofibrillar protein, Current Research in Food Science 9 (2024) 100814. https://doi.org/10.1016/j.crfs.2024.100814.

[84] X. Qin, C. Yang, J. Si, Y. Chen, J. Xie, J. Tang, X. Dong, Y. Cheng, X. Hu, Q. Yu, Fortified yogurt with high-quality dietary fiber prepared from the by-products of grapefruit by superfine grinding combined with fermentation treatment, LWT 188 (2023) 115396. https://doi.org/10.1016/j.lwt.2023.115396.

[85] J. Luo, Y. Wang, H. Guo, F. Ren, Effects of Size and Stability of Native Fat Globules on the Formation of Milk Gel Induced by Rennet, Journal of Food Science 82 (2017) 670–678. https://doi.org/10.1111/1750-3841.13649.

[86] C. Wang, X. Lou, J. Wang, Fatty Acid Composition and Fat Stability of Raw Milk and Pasteurized Milk from Laoshan Goats, JAS 8 (2016) 149. https://doi.org/10.5539/jas.v8n6p149.

[87] H. Zhou, Y. Zhao, D. Fan, Q. Shen, C. Liu, J. Luo, Effect of Solid Fat Content in Fat Droplets on Creamy Mouthfeel of Acid Milk Gels, Foods 11 (2022) 2932. https://doi.org/10.3390/foods11192932.

[88] C. Liu, W. Li, C. Li, X. Zhang, G. Wang, Y. Shen, Y. Wang, X. Liu, L. Sun, Addition of Cyperus esculentus (tiger nut) milk improved the flavor and gelation properties of set yogurt: The main contribution of volatile constituents, starch and proteins, Food Hydrocolloids 155 (2024) 110212. https://doi.org/10.1016/j.foodhyd.2024.110212.

[89] M.K. Hossain, J. Keidel, O. Hensel, M. Diakité, The impact of extruded microparticulated whey proteins in reduced-fat, plain-type stirred yogurt: Characterization of physicochemical and sensory properties, LWT 134 (2020) 109976. https://doi.org/10.1016/j.lwt.2020.109976.

[90] I.C. Torres, J.M. Amigo, J.C. Knudsen, A. Tolkach, B.Ø. Mikkelsen, R. Ipsen, Rheology and microstructure of low-fat yoghurt produced with whey protein microparticles as fat replacer, International Dairy Journal 81 (2018) 62–71. https://doi.org/10.1016/j.idairyj.2018.01.004.

[91] H.-L. Li, L.-X. Su, M.-T. Qiu, Q. Jiang, X.-M. Wang, Z.-C. Tu, Y.-H. Shao, J. Liu, Enhancing the gel properties of whey protein isolate via konjac mannan-crosslinking and their application in non-fat yogurt, LWT 215 (2025) 117282. https://doi.org/10.1016/j.lwt.2024.117282.

[92] Y.-H. Yu, L.-B. Wu, L.-Q. Li, M.-Y. Jin, X. Liu, X. Yu, F. Liu, Y. Li, L. Li, J.-K. Yan, Effect of pectic polysaccharides from fresh passion fruit (Passiflora edulis f. flavicarpa L.) peel on physicochemical, texture and sensory properties of low-fat yoghurt, Food Chemistry 479 (2025) 143801. https://doi.org/10.1016/j.foodchem.2025.143801.

[93]J. Ran, S. Pang, H. Li, R. Zhao, Y. Zhang, Y. Li, M. Yang, Gel properties of mung bean protein-sodium caseinate hybrid yogurt: Physicochemical properties, microstructure, and intermolecular interactions, Food Chemistry: X 24 (2024) 101977. https://doi.org/10.1016/j.fochx.2024.101977.

[94] J. Król, A. Brodziak, L. Ślusarczyk, A. Matwijczuk, M. Chwil, R. Matraszek-Gawron, Yogurt with cornflower (Centaurea cyanus L.) petals as a source of antioxidant compounds and dietary fiber: Physicochemical and spectroscopic research during storage, Journal of Dairy Science 108 (2025) 2243–2263. https://doi.org/10.3168/jds.2024-25628.

[95] D. Cerdá-Bernad, E. Valero-Cases, J.J. Pastor, M.-J. Frutos, Microencapsulated saffron floral waste extracts as functional ingredients for antioxidant fortification of yogurt: Stability during the storage, LWT 184 (2023) 114976. https://doi.org/10.1016/j.lwt.2023.114976.

[96] S. Khubber, K. Chaturvedi, N. Thakur, N. Sharma, S.K. Yadav, Low-methoxyl pectin stabilizes low-fat set yoghurt and improves their physicochemical properties, rheology, microstructure and sensory liking, Food Hydrocolloids 111 (2021) 106240. https://doi.org/10.1016/j.foodhyd.2020.106240.

[97] H. Li, T. Liu, X. Zou, C. Yang, H. Li, W. Cui, J. Yu, Utilization of thermal-denatured whey protein isolate-milk fat emulsion gel microparticles as stabilizers and fat replacers in low-fat yogurt, LWT 150 (2021) 112045. https://doi.org/10.1016/j.lwt.2021.112045.

[98]A. Kharlamova, T. Nicolai, C. Chassenieux, Heat-induced gelation of mixtures of casein micelles with whey protein aggregates, Food Hydrocolloids 92 (2019) 198–207. https://doi.org/10.1016/j.foodhyd.2019.01.048.

[99] H. Du, X. Wang, H. Yang, F. Zhu, J. Cheng, X. Peng, Y. Lin, X. Liu, Effects of mulberry pomace polysaccharide addition before fermentation on quality characteristics of yogurt, Food Control 153 (2023) 109900. https://doi.org/10.1016/j.foodcont.2023.109900.

[100] H. Lesme, C. Rannou, C. Loisel, M.-H. Famelart, S. Bouhallab, C. Prost, Controlled whey protein aggregates to modulate the texture of fat-free set-type yoghurts, International Dairy Journal 92 (2019) 28–36. https://doi.org/10.1016/j.idairyj.2019.01.004.

[101] A. Nazari, S. Zarringhalami, B. Asghari, Influence of germinated black cumin (Nigella sativa L.) seeds extract on the physicochemical, antioxidant, antidiabetic, and sensory properties of yogurt, Food Bioscience 53 (2023) 102437. https://doi.org/10.1016/j.fbio.2023.102437.

[102] S.S. Gite, M. Karmakar, S. Mokashi, C.G. Dalbhagat, V. Kambhampati, R.K. Raigar, R.M. Shukla, Exploration of simulated human olfactory system and its integration with machine learning algorithms for food quality assessment: A review, Trends in Food Science & Technology 159 (2025) 104977. https://doi.org/10.1016/j.tifs.2025.104977.

[103] V. Nemati, R. Mozafarpour, Exopolysaccharides isolated from fermented milk-associated lactic acid bacteria and applied to produce functional value-added probiotic yogurt, LWT 199 (2024) 116116. https://doi.org/10.1016/j.lwt.2024.116116.

[104] J. Jiang, Y. Jiang, H. Li, D. Zhu, Y. He, L. Yang, S. Wang, J. Liu, Y. Zhang, H. Liu, Application of soybean isolate protein (SPI) and soy hull polysaccharide (SHP) complex in fermentation products, International Journal of Biological Macromolecules 258 (2024) 128806. https://doi.org/10.1016/j.ijbiomac.2023.128806.

[105] J. Yang, J. Sun, J. Yan, X. Zhang, Y. Ma, C. Liu, P. Du, A. Li, Impact of Potentilla anserine polysaccharide on storage properties of probiotic yak yoghurt, International Dairy Journal 141 (2023) 105585. https://doi.org/10.1016/j.idairyj.2023.105585.

[106] M. Tian, J. Cheng, H. Wang, Q. Xie, Q. Wei, M. Guo, Effects of polymerized goat milk whey protein on physicochemical properties and microstructure of recombined goat milk yogurt, Journal of Dairy Science 105 (2022) 4903–4914. https://doi.org/10.3168/jds.2021-21581.

[107] J. Cheng, S. Xie, Y. Yin, X. Feng, S. Wang, M. Guo, C. Ni, Physiochemical, texture properties, and the microstructure of set yogurt using whey protein–sodium tripolyphosphate aggregates as thickening agents, J Sci Food Agric 97 (2017) 2819–2825. https://doi.org/10.1002/jsfa.8110.